Department of Precision and Microsystems Engineering

Design of a Hybrid Tunable Magnet Actuator with increased dynamic capabilities

T.R. Swank

Report no : 2023.048
Coach : Dr. S.H. Hossein Nia Kani
Professor : Dr. S.H. Hossein Nia Kani
Specialisation : Mechatronic System Design
Type of report : Master Thesis
Date : 7 July 2023

DELFT UNIVERSITY OF TECHNOLOGY - DEPARTMENT OF PRECISION AND MICROSYSTEMS ENGINEERING

Design of a Hybrid Tunable Magnet Actuator with increased dynamic capabilities

Tim Swank

July 17, 2023

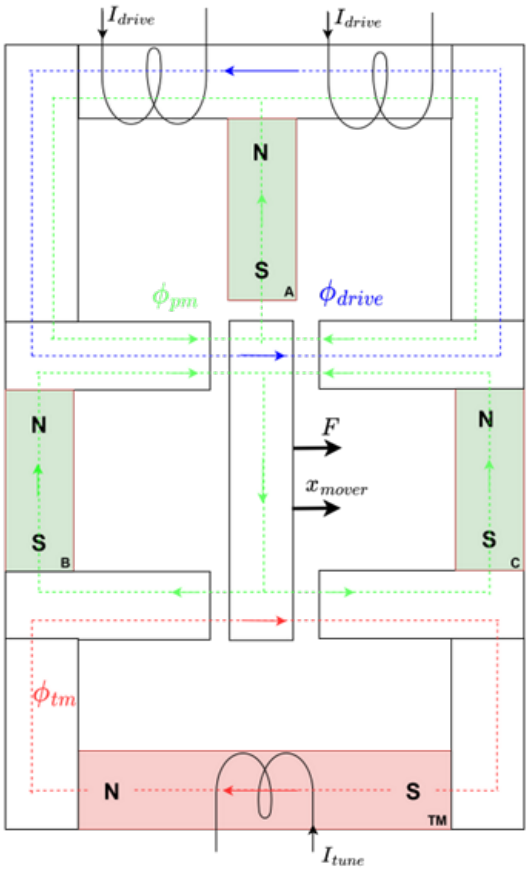

Coach: Dr. S.H. Hossein Nia Kani

PREFACE

First, I would like to thank Hassan for all the feedback and fun engineering discussions the past year. They have helped to keep me on the right track and kept me motivated to show the results of my work.

Next, I would like to thank the people close to this project: Jo, Yorick, Endre, Leon and Bochen for their feedback and support during our regular meetings.

I would like to thank the other students present in the Monday meetings, I have learned a lot from your presentations and your feedback on mine.

A special thanks to Max, Bruno, Maxime and Emie for the many lunches and coffee breaks that made the year much more enjoyable.

Finally, I would like to thank my parents that have shown unconditional support throughout my studies and all projects around it. Without them, I would not have been where I am today.

T.R. Swank
Delft, July 2023

SUMMARY

To increase the accuracy of high-precision motion systems, the heat dissipation in electromagnetic actuators must be reduced to limit thermal expansion.
Variable Reluctance Actuators have a high-frequency bandwidth but suffer from heating when providing high forces for sustained periods.
Tunable Magnet Actuators (TMA) can provide a force endlessly without the need for constant energy input. This is done by in-situ tuning of the remanent magnetic flux density of a low coercivity permanent magnet that provides the magnetic field instead of a drive coil. The TMA is theoretically capable of changing its output in $1ms$, limited by the magnetic diffusion time of the AlNiCo 5 magnet, resulting in an operational frequency bandwidth of $f_{bw,max} = 100Hz$. However, changing the force output requires significant energy input. Therefore, this approach is only beneficial for following low-frequency signals of up to $f_{bw,eff} = 1Hz$. Finding a solution to deal with the limited efficient frequency bandwidth of the TMA is therefore a logical next step for the TMA.
In this thesis project, the chosen strategy to address the problem is the integration of a Reluctance actuator with a tunable magnet actuator. This approach aims to achieve efficient low-frequency actuation while also allowing the tracking of high-frequency signals. By combining these two elements, a notable reduction in heat dissipation can be achieved, mainly when the signal contains a low-frequency component or is offset like in a gravity compensator application.
An obvious solution would be to either add a drive coil to the existing HTMA design by W. Hoekwater or connect the HTMA in parallel with an HRA as proposed by E.P. Ronaes. However, this research proposes an elegant actuator design that integrates a drive coil and a tunable magnet in a single magnetic circuit, both acting on the same mover but separated by permanent magnets (NdFeB) that provide a bias flux for both. This increases the motor constant and linearizes the actuator characteristics. The design is shown in figure 0.1.
Using the Magnetic Equivalent Circuit method and the Maxwell stress tensor, the actuator is characterized. The result is shown in figure 0.2 where the motor characteristic line is shifted up and down due to the tuning of the magnet. Then, using COMSOL Multiphysics, a more detailed design is analyzed. The results show a 12.4N/A motor constant for the drive coil and a 12.2N/T motor constant for the Tunable magnet. Correction factors are added to account for magnetic non-idealities that influence the magnet tuning. The Dynamic HTMA allows for the tracking of high-frequency signals. When compared to a conventional reluctance actuator it has much less heat dissipation if the signal is offset and for the same energy input, the force range is larger.

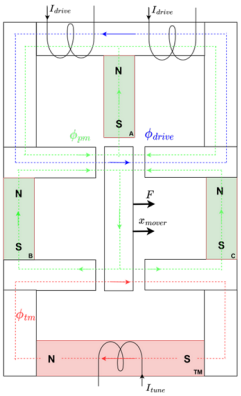

Figure 0.1: Dynamic Tunable Magnet Actuator

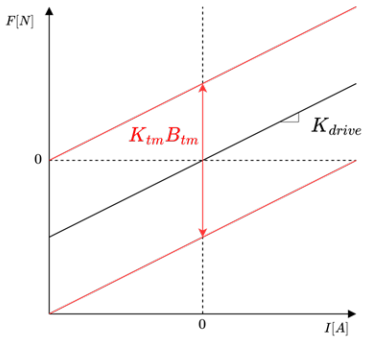

Figure 0.2: Actuator Characteristics of a combined Hybrid Tunable magnet actuator at x=0

CONTENTS

LIST OF FIGURES

LIST OF TABLES

1. Introduction

1.1. Motivation

Electromagnetic actuators are widely used in precision mechatronic systems [12]. They rely on an electromagnetic coil to generate the magnetic flux that leads to a magnetic attraction force between a mover and a stator. However, with the current that flows through the coil comes Joule heating. This heat dissipation causes thermal expansion of the actuator components. Especially in vacuum environments where convective cooling is not possible. For quasi-static applications that provide a force over longer periods of time, this is a significant issue because it degrades the nanometer precision of the actuator. To counter this, the Tunable Magnet Actuator project was started at the TU Delft in 2017. The goal of this project is to develop a high-efficiency electromagnetic actuator based on magnetization state tuning with negligible heat generation when operated in quasi-static mode[13].

For many years, Lorentz force actuators have been the industry standard due to their linear force-current relation and low stiffness. However, the development of Variable Reluctance actuators (RA) has shown that their force density can be up to 10x higher than Lorentz actuators. Because of their non-linear force-current relation, advanced control is required [14]. In order to allow for linear controllers, Hybrid Reluctance Actuators (HRA) have been developed that use a permanent magnet to provide a bias flux which can provide a more linear force-flux relation.

The Tunable Magnet actuator (TMA) works to the same principle as Reluctance Actuators but replaces the flux-inducing coil with a low coercivity AlNiCo magnet. To control the force output, the strength of the magnet can be tuned using a short current pulse. After tuning, the TMA requires no energy input to maintain its force output, significantly reducing heat dissipation.

Examples of application areas that profit from more efficient actuators are high precision positioning stages such as gravity compensators (figure 1.1a) and Deformable mirrors (figure 1.1b) as the gravitational force is quasi-static and adaptive optics are often used in vacuum conditions like satellites or EUV lithography machines.

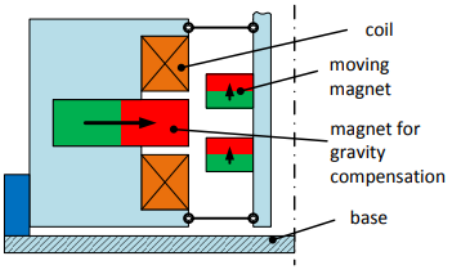

(a) A Magnetic Gravity Compensator by Hüfner [3].

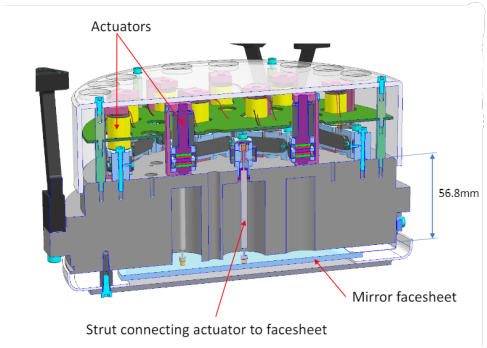

(b) A Deformable mirror Designed by TNO [15].

Figure 1.1: Example applications where tunable magnets can provide a benefit.

1.2. Prior Art

The concept of Magnetization state tuning has been applied in various applications and Vietor [7] subdivided this into the following categories:

1. Magnetic Clamping
2. Flux weakening or boosting in electric motors
3. Magnetic gearing
4. Magnetic actuation

Applications in the Magnetic clamping category use an electro permanent magnet. Meaning the magnet is switched on or off by fully magnetizing and demagnetizing the magnet. An example is shown in figure 1.2 as designed by Knaian [16]. The tuning process is simple as the 'on' state can be reached by saturating the magnet in either direction. A complex algorithm is not required because it is effective as long as the saturation threshold is exceeded.

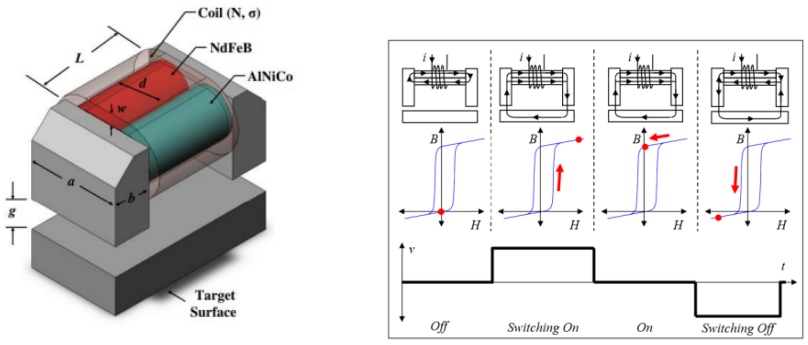

(a) A CAD model of the Electropermanent Actuator by Knaian [16]

(b) The schematic working principle of the EPM Actuator [16]

Figure 1.2: An energy-efficient Electropermanent Actuator

This clamping mechanism currently only supports 2 force levels. To use it as an actuator, a variable force is desired. Hufner [3] proposes a Gravity Compensator where an AlNiCo magnet is variably tuned with a 3-step process to deliver a variable force. Tuning of the magnet is done using predetermined current pulses as shown in figure 1.3.

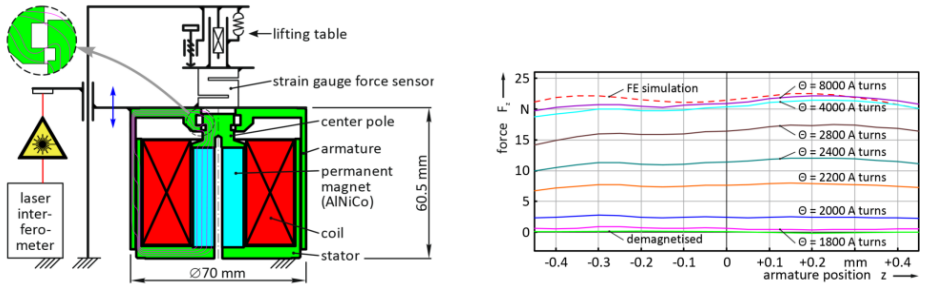

(a) A schematic section drawing of the MGC.

(b) The force output levels as a result of increased current pulses.

Figure 1.3: The schematic working principle of the Magnetic Gravity Compensator [3]

This open-loop tuning process is limited as it is unable to deal with changes in the system and is

only able to reach the correct state from a demagnetized state. To enable the implementation of in-situ magnetization state tuning for a broader range of applications, Vietor [7] developed a novel tuning algorithm, and modeled, designed, and validated the first Tunable magnet actuator. This is introduced in section 2.

1.3. Problem Definition

The TMA is theoretically capable of changing its output in $1ms$, limited by the magnetic diffusion time of the AlNiCo 5 magnet. To avoid aliasing and have sufficient phase margin at unity-gain cross-over frequency [12] states that the sampling rate should be about 10 times the control bandwidth, resulting in an operational frequency bandwidth of $f_{bw,max} = 100Hz$. However, tuning the magnet itself requires significant energy input. In order to assess whether it is beneficial to use a TMA over a conventional RA, a metric was introduced by [16], called the Break-even Tuning Interval (BTI) which is shown in eq. 1.1. E_{hyst} are the hysteresis losses inside the permanent magnet during tuning and $E_{TM,copper}$, is the energy dissipation in the tuning coil. P_{EM} is the continuous energy dissipation of a comparable reluctance actuator.

$$T_{be} = \frac{E_{hyst} + E_{TM,copper}}{P_{EM}} \tag{1.1}$$

BTI calculations by [7] and [4] show that the TMA is only beneficial for following low-frequency signals of up to $f_{bw,eff} = 1Hz$. Finding a solution to deal with the limited efficient frequency bandwidth of the TMA is therefore a logical next step for the TMA. This work builds on prior work from [7], [4], [1] and [2] and aims to improve the Tunable Magnet technology by expanding the dynamic capabilities of the Tunable Magnet Actuator. The chosen strategy to address the problem is the integration of a Reluctance actuator with a tunable magnet actuator. By combining these two elements, a notable reduction in heat dissipation can be achieved, mainly when the signal contains a low-frequency component, is offset, or requires compensation for drift. An example of this can be seen in figure 1.4, where a dynamic force in blue is provided by a reluctance actuator, and static offset force is provided by the tunable magnet in green. If these outputs are added together, the combined actuator output is more efficient than when a single reluctance actuator has to provide the red profile on its own. In Appendix C, a 1st-order approximation is made of how much the heat dissipation could be reduced by using a combined actuator force output as shown in figure 1.4.

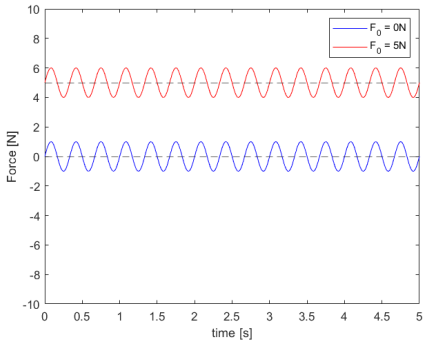

(a) A force profile executed with a Reluctance actuator with a constant bias force of $F_0 = 0N$ and $5N$.

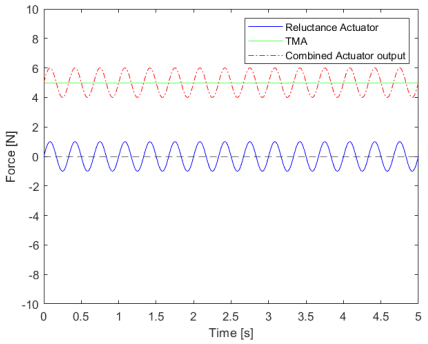

(b) The offset and dynamic force components are split, but the combined output is the same. Therefore, the RA operates in a much more efficient force range.

Figure 1.4: An illustration of the split in low- and high-frequency signals.

1.4. Research Goal & Objectives

This research aims to further develop the Tunable Magnet Actuator to reduce heat dissipation in high-precision applications. Therefore the goal of this thesis project is:

Develop a Hybrid Tunable Magnet Actuator that is capable of high-frequency actuation with low heat dissipation

To achieve this, the following objectives are defined:

1. Develop a concept that combines a tunable magnet and a drive coil that maximizes the motor constants to minimize heat dissipation.
2. Model the actuator with a 1st-order model to prove the functionality and illustrate the actuator characteristics.
3. Develop more detailed 3D model that can be analyzed with a finite element model to provide the motor constants, study non-idealities that can affect the operation of the actuator, and prove the benefit of this actuator compared to a conventional reluctance actuator that has a similar motor constant.
4. Develop a simple control algorithm and build a test setup to verify the FEA results and validate the concept.

1.5. Thesis Outline

First, in section 2, the theory on permanent magnet modeling and magnetization state tuning is introduced. This section can be skipped if you are familiar with this topic. Section 3 is the main contribution in the form of a scientific paper. It is set up to be read independently and will therefore have some overlap with this introductory chapter. It does refer to the appendices of this report for further reading. Conclusions and recommendations of the thesis are elaborated in section 4. Appendix A gives more details on the design process, Appendix B describes the plans for the experimental setup, Appendix C Shows a preliminary calculation on the benefits of separating the low- and high-frequency forces and Appendix D gives context on existing combined actuators found in the literature.

2. PRELIMINARY

This section describes the theoretical background of magnets, magnetic circuits, and their combination to form an electromagnetic actuator.

2.1. Permanent magnets

A magnetic field H is produced by an electrical current as described by Ampere's law.

$$\oint \boldsymbol{H} \cdot d\boldsymbol{l} = I_{tot} \tag{2.1}$$

This can be either from electrical current through a wire or on a quantum level through the movement of electrons inside atoms. The magnetic field can be described by the flux density B in units of Tesla. B and H are related to each other by the material property of μ_0 which describes the magnetic permeability of a material. The flux density in the magnet can be found with equation 2.2, where H is the externally applied field and M is the magnetization state of the magnetic material itself.

$$B_m = \mu_0 (H + M) \tag{2.2}$$

Ferromagnetic materials such as iron can be magnetized when exposed to an external magnetic field. This exposure can align the magnetic fields of small subdomains inside the material. When aligned in the same direction, the material becomes a magnetic dipole with a north and south pole. The magnetization process is not linear and has a hysteretic character that can be visualized by plotting B against H. This magnetization process is presented in figure 2.1. When a magnet is first magnetized, it will follow the so-called virgin curve up to the saturation point.

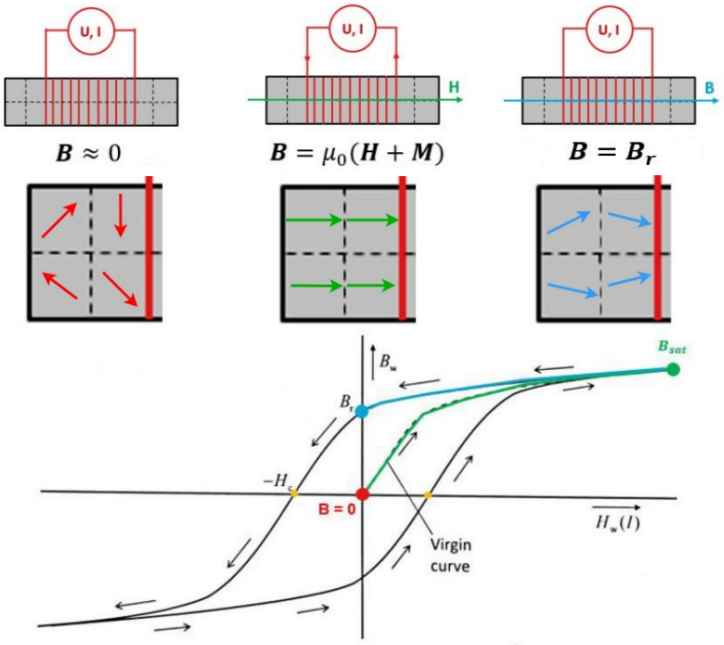

Figure 2.1: 3 different Magnetization states of a ferromagnetic material [4].

The B-H curve shown in figure 2.1 shows the Major Hysteresis loop that determines the outermost operation boundaries of a magnetic material. It is important to note that changes to the magnetic

state adhere to Madelung's rules, for example, they are history-dependent and loops can only be traversed counter-clockwise [6]. When the magnet is demagnetized past the 'Knee point' and the applied field H_m is removed, the magnet will follow the recoil line trajectories as shown in figure 2.2a. Furthermore, Figure 2.2b shows that Minor loops can be followed within the Major loop curve.

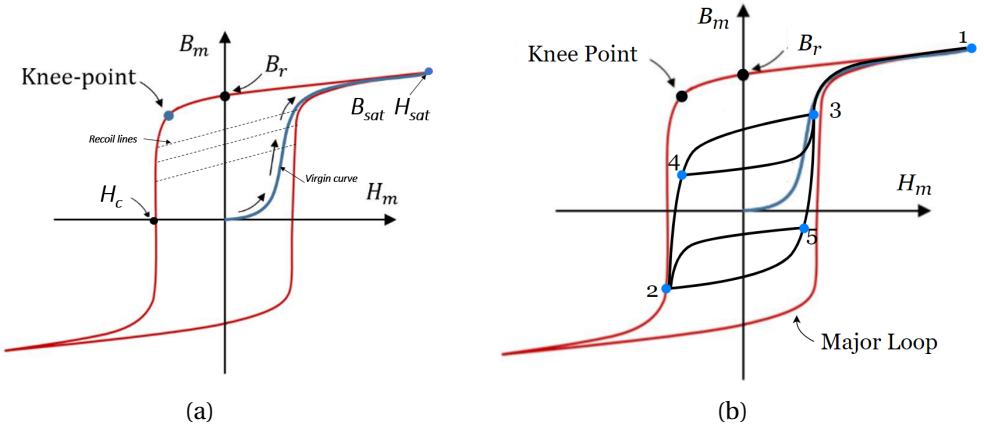

Figure 2.2: (a)The Major loop with its recoil lines. (b)Minor loops are followed when operating within the Major loop boundaries.

2.2. Magnetic circuits

The magnetic permeability of iron is much higher than air, up to 200000 times higher for soft iron. Therefore, an iron core or 'yoke' can be used to concentrate and direct the magnetic field for our benefit, for example from a coil to an air gap in an actuator.

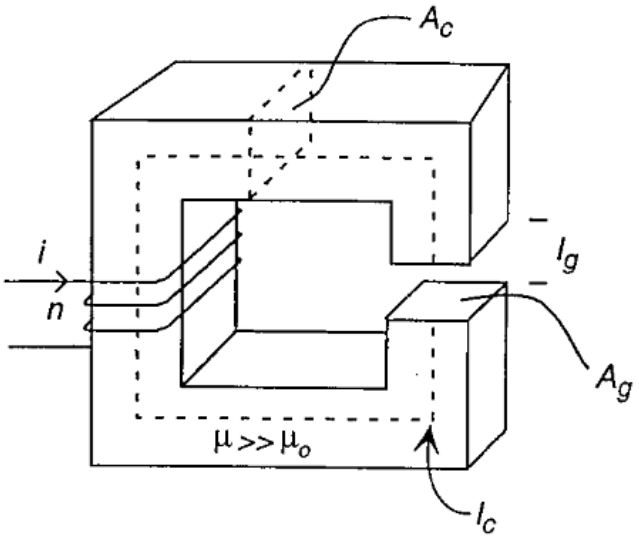

Figure 2.3: A simple magnetic circuit with a coil and a single air gap [5]

The magnetic flux density in the air gap as a result of the current applied to the coil can be calculated by Ampere's and Gauss' law:

$$\oint \boldsymbol{H} \cdot d\boldsymbol{l} = nI \tag{2.3}$$

or

$$H_c l_c + H_g l_g = nI \tag{2.4}$$

Assuming no flux losses, Gauss' law states that flux throughout the circuit must be conserved:

$$B_m A_m = B_g A_g \tag{2.5}$$

Making use of the known BH relations for air/vacuum: $B_g = \mu_0 H_g$ and $B_c = \mu H_c$ we can use equations 2.3, 2.4 and 2.5 to derive:

$$B_g = \frac{nI}{\frac{A_g}{A_c}\frac{l_c}{\mu} + \frac{l_g}{\mu_0}} \tag{2.6}$$

Assuming that $A_g \approx A_c$ and $\mu \gg \mu_0$ this can be reduced to:

$$B_g = \frac{nI\mu_0}{l_g} \tag{2.7}$$

The example shows a simple case, but this derivation can be difficult for more complex magnetic circuits. Therefore, the circuit can be modeled as a lumped-parameter model with a magnetic source, magnetic resistances, and magnetic flux. This magnetic equivalent circuit method (MEC) can be seen as an analog to the electrical lumped parameter model as shown in figure 2.4 and table 2.1

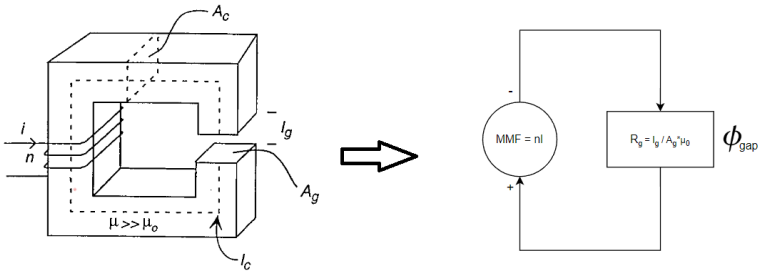

Figure 2.4: The Magnetic Equivalent circuit representation of the Magnetic circuit shown in figure 2.3 with a coil and a single air gap

Electric circuit		Magnetic circuit	
current	$I = \frac{V}{R}$	flux	$\phi = \frac{MMF}{R}$
current density	$J = \frac{1}{A}$	flux density	$B = \frac{\phi}{A}$
resistance	$R = \frac{\rho l}{A}$	reluctance	$R = \frac{l}{\mu A}$
voltage	V	magnetomotive force	$MMF_c = nI$ $MMF_{pm} = H_m L_m$

Table 2.1: Magnetic equivalent circuit comparison to the electric circuit lumped parameter model.

Using the equations provided in table 2.1 we can again calculate the magnetic flux density in the gap as a result of the current applied to the coil:

$$B_g = \frac{\phi_{gap}}{A_g} = \frac{MMF_c}{RA_g} = \frac{nI}{RAg} \tag{2.8}$$

The reluctance of the air gap can be approximated by:

$$R = \frac{l_g}{\mu_0 A_g} \tag{2.9}$$

Combining equation 2.8 and 2.9 we find:

$$B_g = \frac{nI\mu_0}{l_g} \tag{2.10}$$

When electric and magnetic circuits become more complex, these derivations become too long to do by hand. Kirchhoff's Loop rule and junction rule can be used to set up a set of linear equations that can easily be solved with linear algebra. An example of such a circuit is shown in figure 2.5.

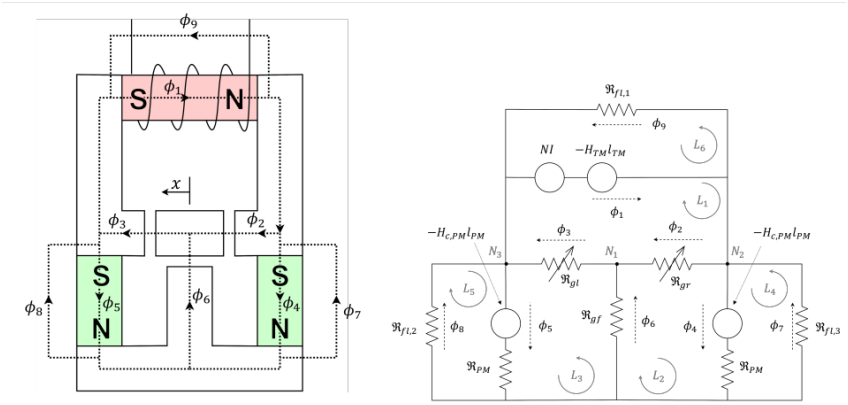

Figure 2.5: A Magnetic equivalent circuit of the Hybrid Tunable magnet actuator. [2]

2.3. Variable Reluctance Actuators

Variable Reluctance actuators generate their force through the magnetic attraction between 2 ferromagnetic materials inside a magnetic field generated by a permanent magnet, a coil, or a combination of both.
A common reluctance actuator design is in the form presented in figure 2.6.

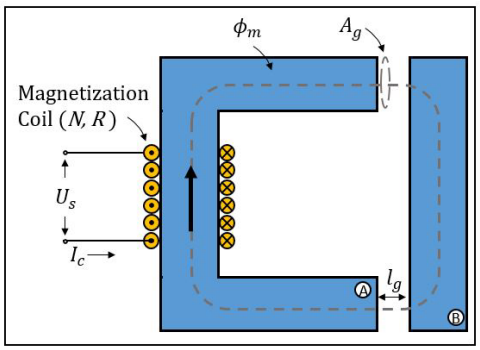

Figure 2.6: A C-shape Reluctance actuator [4]

To find the force produced by this actuator, we can use the Maxwell Stress tensor [5] (equation 2.11). It relates the force to the magnetic flux density in the air gap B_g. This can be found with the lumped-parameter model this time considering 2 air gaps of identical length. (equation **??**.

$$\boldsymbol{F} = \frac{1}{2\mu_0} \oint B_n^2 \boldsymbol{n} ds = \frac{B_g^2 A_g}{\mu_0} \tag{2.11}$$

Equation 2.11 shows us that the force relates non-linear to the control input parameter: current I. While advanced modeling, smart control strategies, and other linearization methods [14] can be used to negate this as much as possible, the intrinsic non-linearity is undesired.
The hybrid Reluctance actuator (HRA) is an evolution of this design. By using a permanent magnet to create a bias force and a different layout, the force flux relation can be linearized. A schematic overview of an HRA is shown in figure 2.7. A bias flux, shown by the green dashed line, is created by a PM, shown in green. A control flux, shown by the blue dashed line, is created by the coils. In the left gap, the fluxes sum up while in the right gap, the fluxes subtract. Thereby, a linear relationship between the flux and the force is obtained.

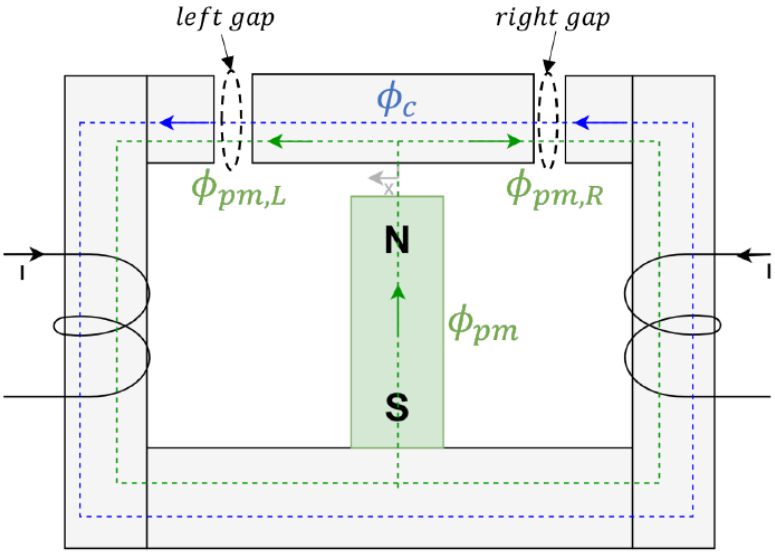

Figure 2.7: A schematic overview of an HRA. [1]

We can again calculate the flux in the gaps with the lumped parameter model. The Flux in the gaps can be calculated from the coil and permanent magnets. With the current direction as defined in figure 2.7 the total flux density in the left air-gap is $B_{g,pm} + B_{g,c}$ and in the right gap it equals $B_{g,pm} - B_{g,c}$ [12].

$$B_{g,pm} = \frac{B_r A_p m}{4 A_g} \tag{2.12}$$

$$B_{g,c} = \frac{nI\mu_0}{l_g}\phi_c = \frac{nI\mu_0 A_g}{l_g} \tag{2.13}$$

For this actuator the force current relation can again be calculated with the Maxwell stress tensor [1]:

$$F = \frac{\left(\phi_{pm,L} + \phi_c\right)^2 - \left(\phi_{pm,R} - \phi_c\right)^2}{2\mu_0 A_g} \tag{2.14}$$

Equation 2.14 can be simplified by rewriting the fluxes in the left and right gaps as a function of the flux in the permanent magnet and even further by defining a motor constant K_m and an actuator stiffness k_a to show the force current relation is linear to the control input and is position dependent (equation 2.16).

$$\phi_{pm,L} = \frac{l_g + x}{2l_g}\phi_{pm}, \phi_{pm,R} = \frac{l_g - x}{2l_g}\phi_{pm} \tag{2.15}$$

$$\begin{aligned} F &= \frac{\phi_{pm}}{\mu_0 A_g}\left(\phi_c + \phi_{pm}\frac{x}{2l_g}\right) \\ F &= K_m I + k_a x \end{aligned} \tag{2.16}$$

This development has unlocked a lot of potential to replace the established Lorentz actuators in applications such as deformable mirrors [8].

2.4. Tunable Magnet Actuators

By replacing the coil from the reluctance actuator with a coil and PM combination, an extra subsystem is added. Contrary to the derivations shown in section 2.3, the current is not directly related to the actuator force output anymore. The current is now used to change the remanent flux density of the PM as explained in section 2.5. Therefore to control the force output of the actuator, the flux in the gap is now considered to be its input control parameter. The force-flux relation of the C-shaped TMA (figure 2.8) is given by equation 2.17.

$$\mathbf{F} = \frac{\phi_g^2}{\mu_0 A_g} = \frac{B_g^2 A_g}{\mu_0} = \frac{\mu_0 n^2 I^2 Ag}{4 l_g} \tag{2.17}$$

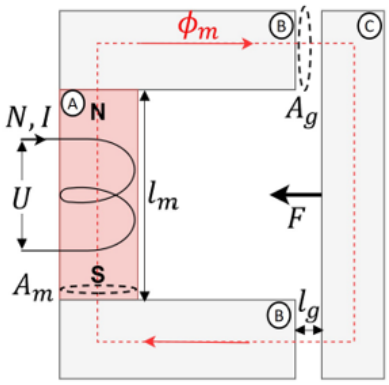

Figure 2.8: C-shaped Tunable magnet actuator as designed by Vietor [2]

In line with the work done by Ito [17] to linearize the reluctance actuator, Hoekwater proposes the same method of linearizing the TMA by using bias fluxes from PMs. The magnetic circuit layout must be optimized for the TMA because if the PM would be placed in the middle like in the HRA design, the Tunable magnet flux would bypass the mover. The essence of the linearization method can be seen in figure 2.9

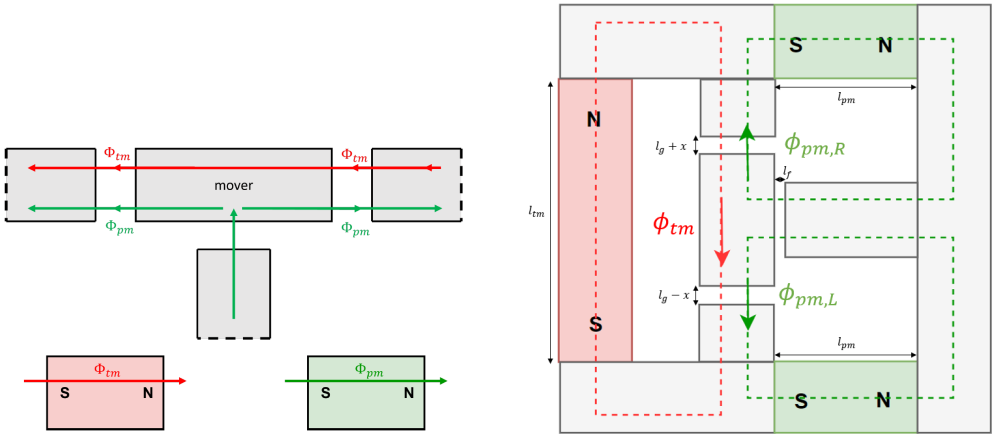

(a) (b)

Figure 2.9: (a)Linearization method with required flux directions. (b) The resulting design of the Hybrid Tunable Magnet Actuator.[1]

Using the lumped parameter model and superposition for the two magnetic circuits, the following force flux relation can be found:

$$\begin{aligned} F &= \frac{\left(\phi_{pm,gL}+\phi_{tm}\right)^2-\left(\phi_{pm,gR}-\phi_{tm}\right)^2}{2\mu_0 A_g} \\ &\approx \frac{2\phi_{pm}}{\mu_0 A_g}\left(\phi_{tm}+\phi_{pm}\frac{2x}{2l_g+\mu_0 A_g \mathscr{R}_{tm}}\right) \end{aligned} \tag{2.18}$$

Where again, this can be simplified to the following force flux relation that is linear:

$$F = K_m\phi_{tm} + k_a x \tag{2.19}$$

Ronaes showed that the original lumped parameter model could be improved by modeling the complete circuit instead of using the superposition of 2 separate circuits. This showed that unlike previously assumed, the flux in the tunable magnet is also a function of the position of the mover. That dependency can be used to compensate during the tuning process by relating it to the middle position of the mover:

$$B_{gr} = \frac{\partial B_{gr}}{\partial x}x + B_{gr,x_0} \tag{2.20}$$

2.5. Magnetization State Tuning Algorithms

"The main challenge in implementing the TM concept is to determine the correct coil current to tune the magnet to the desired strength." – Vietor [7]
Section 2.3 shows how the magnetic flux in the gap is determined from a coil and from a permanent magnet and how the operating point of the PM is derived. In order to 'tune' the magnet, the operating point needs to be changed accordingly to reach a different flux level. The operating point of a permanent magnet B_m is dependent on any external applied magnetic field (by a coil) and the circuit it is placed in. This is described by its Hysteresis curve and the load line [5].
For the example actuator shown in figure 2.8 the method from the previous subsection can be used to find equation 2.21. In combination with the Hysteresis curve of the PM, this equation can then be

used to find the operating point as visualized in figure 2.10. The Operating point of the magnet is the intersection of the load line and the BH curve of the magnet.

$$B_m = -\mu_0 \frac{A_g l_m}{2 A_m l_g} \left(H_m - \frac{NI}{l_m} \right) \tag{2.21}$$

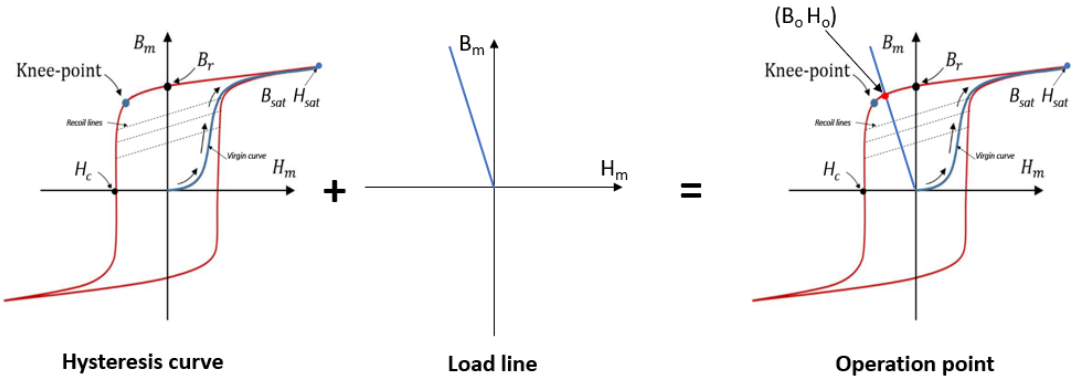

Figure 2.10: Operation point of a magnet in a magnetic circuit. [1]

If the operating point needs to be changed, this can be done with a current pulse on the coil and can be described by a shift in the load line. This process is illustrated in figure 2.11. When the applied current is removed, the magnetic flux density will return to its remanent state which lies along the unshifted load line.

$$B_m = -\underbrace{\mu_0 \frac{k_2}{k_1} \frac{A_g l_m}{2 A_m l_g(x)}}_{\text{slope}} (H_m - \underbrace{\frac{NI}{l_m}}_{\text{shift}}) \tag{2.22}$$

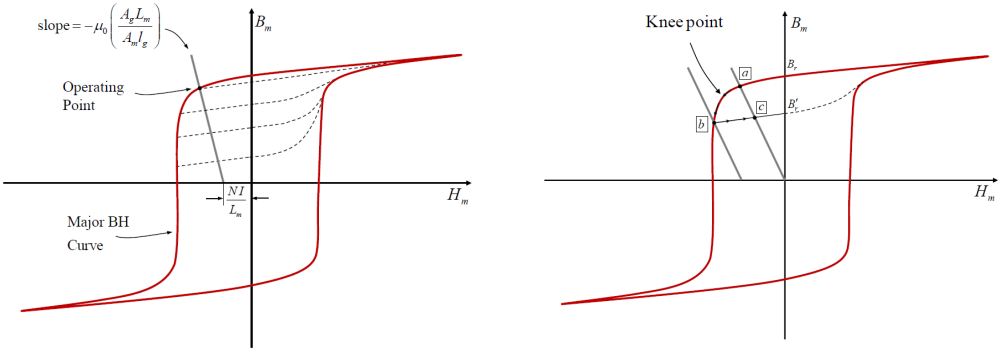

Figure 2.11: (a)Operating point can be changed by shifting the load line through an applied current to the coil. (b) The PM is demagnetized from point a to b. When the current is removed, the operating point follows the recoil line to a new remanent state c

A key part of the Tunable Magnet actuator concept is the ability to control the remanent flux density of the magnet. This is considered one of the biggest challenges in this project [7] as the tuning process is non-linear, history dependant, and rate dependent.
4 methods have been proposed to accurately increase or decrease the magnet remanent state.

Saturation Magnetization State Tuning - SMST
The first method proposed by Vietor [7] is the SMST method. The steps are shown in figure 2.12 below. and consists of 4 states:

1. Off - This is the initial state.
2. Saturate - Positive current is applied to the coil, and the load line shifts right until B_{sat} is reached
3. Demagnetize - Negative current is applied to the coil, and the load line shifts left until the desired 'Corner Point' is reached (B_c).
4. Decay - The current is released and the operation point will shift along the recoil line to the new remanent state.

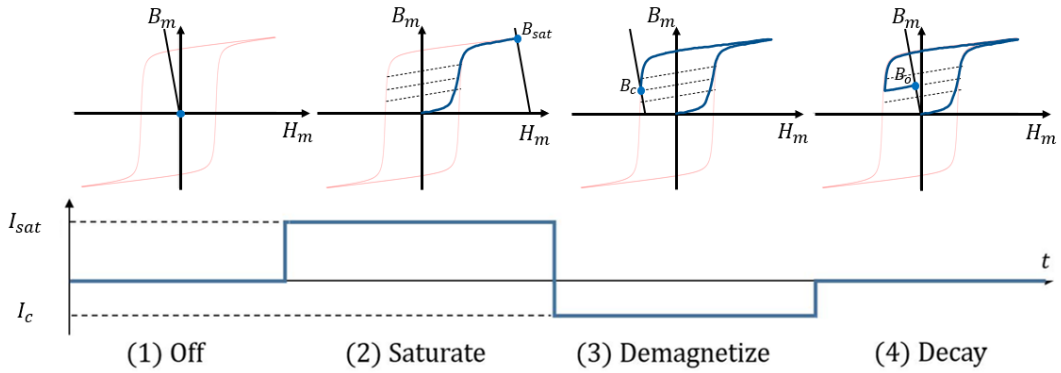

Figure 2.12: The 4-step SMST process to achieve the desired operating point. [1]

- If an increase in remanent flux is desired, an internal minor loop curve is followed until saturation. Followed by demagnetization to a new (higher) corner point via the major loop.
- If a decrease in remanent flux is desired, there is no need for saturation. Instead, the magnet can be demagnetized directly to a new (lower) lower corner point.

Accuracy is high because the every tuning step the known major loop is reached. However, the SMST is not very efficient as for any increase in strength, the saturation step is required.

Minor-loop Magnetization State Tuning MMST
Meijer [4] proposed the MMST method that does not require the saturation step for increasing the magnet strength. This method is theoretically the most efficient method as no more tuning or current is used than required to reach a given magnetization state. The steps are again listed below and illustrated in figure 2.13

1. Off - This is the initial state.
2. Magnetize - Positive current is applied to the coil, the load line shifts right until the desired B_c is reached
3. Decay - The current is released and the operation point will shift along the recoil line to the new remanent state.

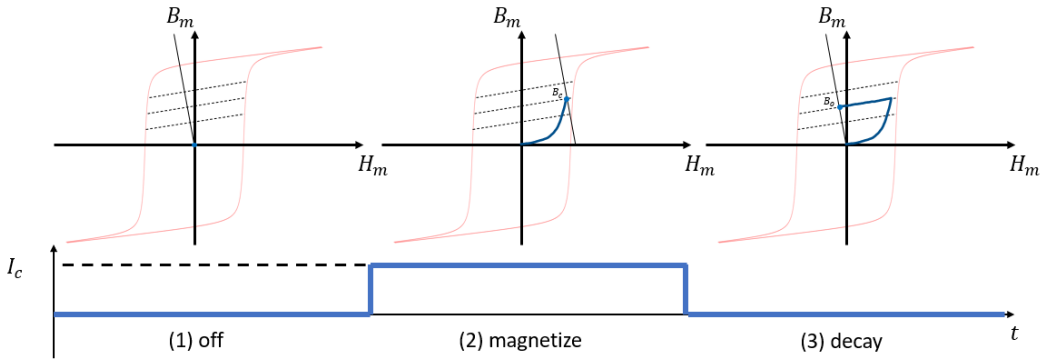

Figure 2.13: The 3-step MMST process to achieve the desired operating point. [1]

The MMST method has proven to be much faster and more efficient but significantly less accurate than the SMST method as the model only contained the major B-H curve data and linearized recoil lines. In practice, the operation point will not reach the Major curve until fully saturated, and therefore inaccuracies are introduced.

Envelope Magnetization State Tuning - EMST

Wiersema [6] showed that the linearizations and simplifications of Vietor and Meijer limited the accuracy and efficiency of the tuning process. A history-dependent and non-linear algorithm was developed to better describe the Hysteresis properties of the magnet. Also, the curves within the major loop are modeled by approximation to more accurately describe the B-H trajectories that the magnet will follow (so-called reversal curves) when magnetized from any remanent state. Figure 2.14b shows the conclusion of his research with accuracy in the left column and Energy usage in the right.

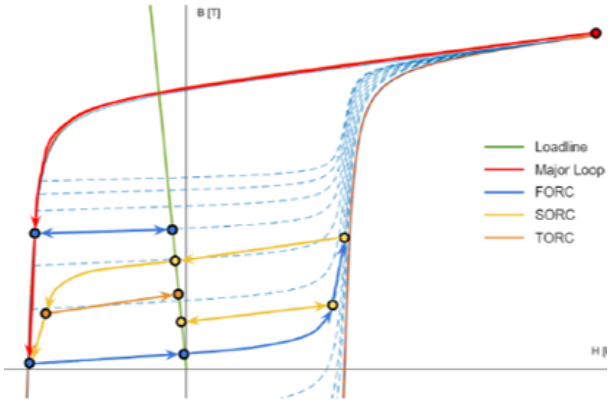

(a)

Magnetization State Tuning		
SMST	5mT	1.25J
MMST	30mT	0.22J
EMST	6mT	0.27J

(b)

Figure 2.14: (a)The Envelope Magnetization State Tuning method with higher order reversal curves. (b) The table shows that it is possible to reach high levels of accuracy without the energy-inefficient saturation step. [6]

Following up on Wiersema, Ronaes [2] has developed an evolution of the MMST method that is based on major loop data and linearization of the recoil curves only. Making use of flux feedback control, the operating point is monitored and when it crosses the recoil line that corresponds to the target remanent state the corner point is reached. This is illustrated in figure 2.15 where the angle α is the

output and β is the reference. This allows for accurate corner point prediction without requiring the data of the reversal curves (drawn in blue).

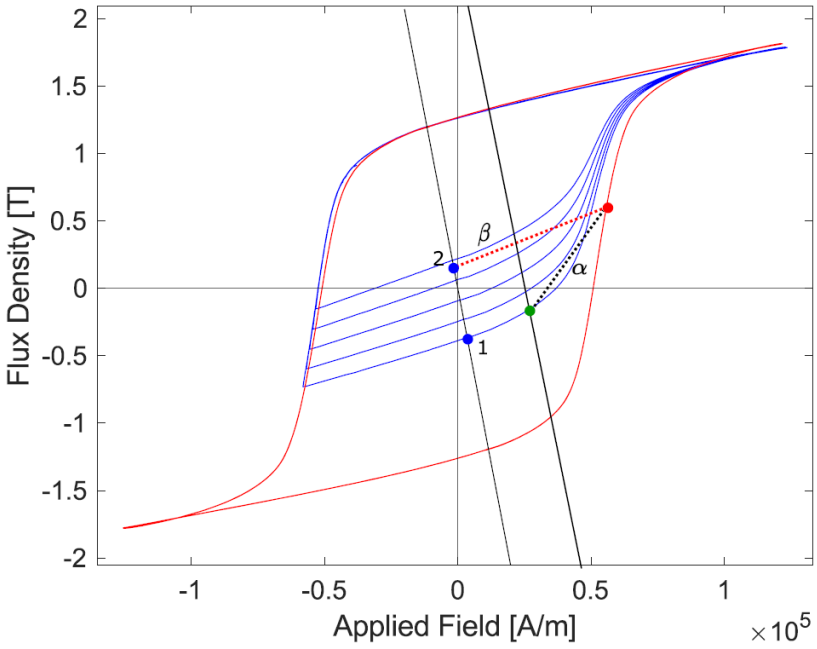

Figure 2.15: Whenever the operation point (green) crosses the linearized recoil line (red dotted line) of the target remanent state 2, the target corner point is reached. [6]

PWM-like Feedback tuning All of the aforementioned methods require prior knowledge of the Major curve and use look-up tables and therefore require a calibration process for each actuator. To circumvent this, Ronaes has designed a PWM-like feedback tuning method that uses a series of short pulses and uses the flux feedback signal to determine if the required remanent flux state is reached or if more pulses are required.

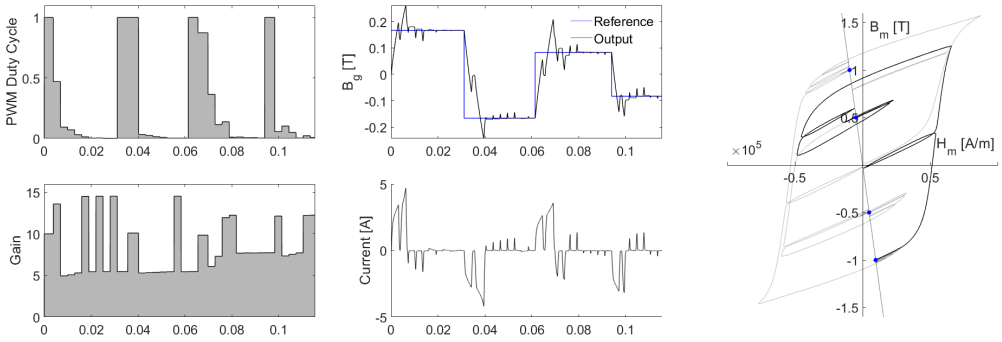

Figure 2.16: Tuning results of PWM-like tuning to four different setpoints. [2]

2.6. Energy dissipation

The purpose of the TMA is to reduce Joule heating through energy consumption reduction. Therefore a performance indicator was conceived to assess in what situations a TMA is more efficient than a conventional Electromagnetic Actuator (EM) for the same actuation force. This is calculated by the Break-Even Tuning Interval (BTI). If the tuning interval is shorter than the BTI, it is more efficient to use a conventional actuator, if it is slower the TMA is more efficient. It is defined as:

$$T_{be} = \frac{E_{hyst} + E_{TM,copper}}{P_{EM}} \tag{2.23}$$

Where E_{hyst} are the hysteresis losses inside the permanent magnet. This can be visualized as the area that is encircled in the B-H curve during the tuning process and calculated by:

$$E_{hyst} = A_M l_m \int H\,dB \tag{2.24}$$

$E_{TM,copper}$, is the joule heating of the coil during tuning where $I(t)$ is the applied current, t the total tuning time and R is the resistance of the Coil.

$$E_{TM,copper} = \int_0^T I^2(t) R\,dt \tag{2.25}$$

Finally, the power dissipation of the EM can be calculated by:

$$P_{EM} = I_{EM}^2 R \tag{2.26}$$

With the most recent designs from Hoekwater and Ronaes BTI values of 1.4s were achieved. Meijer extrapolated his experimentally found values to find a theoretical optimum of 0.29s for the MMST tuning method in his C-Shape actuator design, although further development and optimization would be required to achieve these values. Ultimately the maximum tuning achievable speed is limited by the magnetic diffusion time constant of the permanent magnet, where d_m is the diameter of the magnet and ρ is the electrical resistivity of the magnet material [18].

$$\tau = \frac{d_m^2 B_{sat}}{16 \rho H_{sat}} \tag{2.27}$$

Furthermore, to avoid aliasing and have sufficient phase margin at unity-gain cross-over frequency Schmidt states that the sampling rate should be about 10 times the control bandwidth [12]. This means that to have good performance, the achievable closed-loop bandwidth of a TMA is given by equation 2.28. Reducing the effective bandwidth of the current designs to $f \approx 0.1$Hz.

$$f = \frac{1}{10 T_{be}} \tag{2.28}$$

This means that currently, the TMA is suitable for actuation applications that require quasi-static actuation only

The TMA is relatively efficient compared to reluctance actuators when [7]:

- Large constant bias forces are required
- The tuning magnet is small, due to fewer hysteresis losses
- Tuning times are short

3. Design of a Hybrid Tunable Magnet Actuator with increased dynamic capabilities

This page is left blank intentionally

Design of a Hybrid Tunable Magnet Actuator with increased dynamic capabilities

T.R. Swank

To increase the accuracy of high-precision motion systems, the heat dissipation in electromagnetic actuators must be reduced to limit thermal expansion. Variable Reluctance Actuators have a high-frequency bandwidth but suffer from heating when providing high forces for sustained periods of time. Tunable Magnet Actuators can provide a large force endlessly without the need for constant energy input. The efficient frequency bandwidth of the Tunable Magnet Actuator is a limiting factor, Therefore, a combination of the two techniques is proposed to deliver efficient, high-frequency actuation at a wide range of forces. A design is proposed that integrates a drive coil and tunable magnet into a single magnetic circuit to maximize the motor constants. The new Hybrid Tunable Magnet Actuator allows for tracking of high-frequency signals and has reduced heat dissipation for signals that are offset from zero.

I. Introduction

Variable Reluctance Actuators are widely used in precision mechatronic systems [1]. They rely on a drive coil to generate the magnetic flux to provide magnetic attraction force between a mover and a stator. However, due to the current that flows through the coil windings, these actuators suffer from Joule heating. This heat dissipation causes thermal expansion of the actuator and the components around it. Especially in vacuum environments like space or EUV lithography machines where convective cooling is not possible. For applications that provide a force over longer periods of time like a gravity compensator, this is a significant issue because it degrades the nanometer precision of the system.

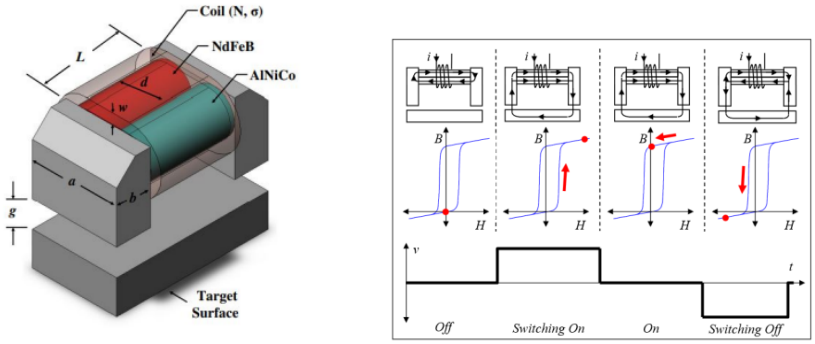

(a) A CAD model of the Electropermanent Actuator by Knaian [2]

(b) The schematic working principle of changing actuator states. [2]

Figure 1. The Electropermanent Actuator

A. State-of-the-art

In order to counteract the joule heating problem, magnetization state tuning is proposed as a solution. Knaian introduced the Electropermanent Actuator [2] that provided an efficient magnetic clamping force. The clamping force is switched on or off by fully magnetizing or demagnetizing a low coercivity AlNiCo magnet using a magnetic field generated by a current pulse from a coil. This allows the device to maintain a constant magnetic attraction force without constant energy input and thus no joule heating after switching on. The principle is shown in figure 1. A complex tuning algorithm is not required because it is effective as long as the magnetic saturation threshold is exceeded. This clamping mechanism only has 2 states, on or off. To use it as an actuator, a continuously variable force is desired. Hufner [3] proposes a

Magnetic Gravity Compensator using a similar concept as [2]. In this device, the magnet is tuned using predetermined current pulses to achieve varying levels of Force output.

To broaden the range of actuator applications, Vietor [4] developed a novel tuning algorithm and introduced the Tunable Magnet Actuator (TMA) making use of the BH relation of the magnet and a linear model of the system. With this novel algorithm, it was possible to tune the AlNiCo5 magnet in situ with an accuracy of 16mT. Meijer [5], Wiersema [6] and Roneas [7] have developed different methods to increase the efficiency of the tuning process. Hoekwater [8] has redesigned the layout of the actuator and implemented NdFeB permanent magnets for bias flux. It has a bi-directional force output and a linear force-flux relation that allows for the use of a linear controller.

B. Problem Statement

The TMA is theoretically capable of changing its output in 1ms, limited by the magnetic diffusion time of the AlNiCo 5 magnet. To avoid aliasing and have sufficient phase margin at unity-gain cross-over frequency, the sampling rate should be about 10 times the control bandwidth, resulting in an operational frequency bandwidth of $f_{bw,max} = 100Hz$ [1]. However, tuning the magnet itself requires significant energy input. In order to assess whether it is beneficial to use a TMA over a conventional RA, a metric was introduced by [2], called the Break-even Tuning Interval (BTI) which is shown in eq. 1. E_{hyst} are the hysteresis losses inside the permanent magnet during tuning and $E_{TM,copper}$ is the energy dissipation in the tuning coil. P_{EM} is the continuous energy dissipation of a comparable reluctance actuator.

$$T_{be} = \frac{E_{hyst} + E_{TM,copper}}{P_{EM}} \tag{1}$$

BTI calculations by [4] and [5] show that the TMA is only beneficial for following low-frequency signals of up to $f_{bw,eff} = 1Hz$. Finding a solution to deal with the limited efficient frequency bandwidth of the TMA is therefore a logical next step for the TMA.

C. Research Contributions

This work builds on prior work from [4], [5], [8], and [7] and aims to improve the Tunable Magnet technology by expanding the dynamic capabilities of the Tunable Magnet Actuator. The chosen strategy to address the problem is the integration of a Reluctance actuator with a tunable magnet actuator. By combining these two elements, a notable reduction in heat dissipation can be achieved, mainly when the signal contains a low-frequency component, or is offset like in a gravity compensator application. An example of this can be seen in figure 2, where a dynamic force in blue is provided by a reluctance actuator, and static offset force is provided by the tunable magnet in green. If these outputs are added together, the combined actuator output is more efficient than when a single reluctance actuator has to provide the red profile on its own. The goal is to achieve low-frequency actuation while also allowing the tracking of high-frequency signals while minimizing heat dissipation. An obvious solution would be to either add a drive coil to the existing HTMA design by W. Hoekwater or connect the HTMA in parallel with an HRA as proposed by E.P. Ronaes. However, this research proposes an elegant actuator design that integrates a drive coil and a tunable magnet in a single magnetic circuit, both acting on the same mover but separated by permanent magnets (NdFeB) that provide a bias flux for both. This allows for a higher motor constant than the solutions mentioned above and linear actuator characteristics to reduce controller complexity.

First, the tunable magnet actuator working principles are further introduced in section II. Next, in section III, the concept of combining the 2 actuators is studied with a lumped-parameter model. Hopkinsons' law is applied to calculate the magnetic flux in the air gaps between the stator and mover. Using the Maxwell stress Tensor, the provided magnetic flux can be related to the force exerted on the mover. Then in section IV, a more detailed design is made in CAD and analyzed with FEM to verify the motor constants and study any non-idealities in the system that may affect the magnet tuning. To validate the concept, the performance is compared to a conventional reluctance actuator with an equal motor constant.

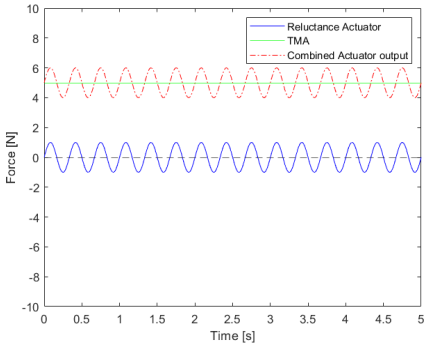

Figure 2. An example of how the low- and high-frequency signals can be separated in a combined actuator

II. Working principles of Reluctance and Tunable magnet actuators

Variable Reluctance Actuators (RA) generate their force through the magnetic attraction between 2 ferromagnetic materials when a magnetic field is present. The variable magnetic field is generated by a drive coil. Next to that, permanent magnets (PM) can be employed to create a bias flux to increase the motor constant and linearize the force-flux relation. In recent work, this kind of actuator is referred to as a 'hybrid' actuator because of its two sources of magnetic fields. The working principle of the Tunable Magnet Actuator (TMA) is very similar to reluctance actuators, however, for its magnetic field generation, it relies on a low-coercivity permanent magnet that can be tuned instead of a drive coil. In order to control the actuator output, a model must be employed to correctly tune the magnet to a desired magnetization state as this will determine the flux in the system and the force exerted on the mover.

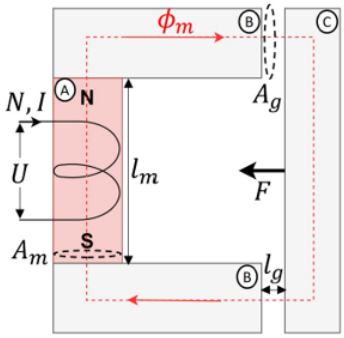

Figure 3. A C-shape Tunable Magnet Actuator [5]

A. Circuit and Permanent Magnet Modeling

The C-shape actuator in fig. 3 designed by [4] and [5] is used as an example. The AlNiCo 5 magnet of length l_m forms the main source of a magnetic field. A tuning coil is placed around the magnet with N windings to provide current pulses for changing the magnetization state. Soft iron yokes (B) and a Mover (C) with cross-section A_g complete the magnetic circuit. The distance between the stator and the mover is denoted by l_g.

The output of the Actuator can be calculated with the Maxwell Stress Tensor [9] in eq. 2.

$$\boldsymbol{F} = \frac{1}{2\mu_0} \oint B_n^2 \boldsymbol{n} ds = \frac{B_g^2 A_g}{\mu_0} \tag{2}$$

where B_n is the magnetic flux density perpendicular to the yokes in the gap area, with n being the normal vector. This gap flux can then be related to the flux density inside the magnet. For permanent magnets, the flux depends on the magnet's operating point (B_m, H_m). The operating point can be determined from the intersection of the load line and

the demagnetization curve of the magnet in the second quadrant of the B-H plane [9]. The load line defines the relation between the flux density inside the magnet and the current applied by the tuning coil while placed inside the circuit. This relation is illustrated in fig. 4

To derive the load line for this circuit, a lumped parameter model is used. Ampere's circuit law describes the conservation of magnetomotive force over the flux path ϕ_m, where H_m and H_g are the respective magnetic field intensities in the magnet and air gaps. The yokes are considered ideal, meaning no MMF is lost between the magnet and the air gaps.

$$H_m l_m + 2H_g l_g = NI_{tune} \tag{3}$$

Gauss' law states that flux throughout the circuit must be conserved. The cross sections of the magnet and air gap are denoted as A_m and A_g

$$B_m A_m = B_g A_g \tag{4}$$

The relation between B_g and H_g for air or vacuum is:

$$B_g = \mu_0 H_g \tag{5}$$

Equation 3, 4 and 5 are combined to derive the load line. Depending on the remanent state of the magnet, the operating point can be found as illustrated in fig. 4(a).

$$B_m = \underbrace{-\mu_0 \frac{A_g l_m}{2A_m l_g(x)}}_{\text{slope}} (H_m - \underbrace{\frac{NI_{tune}}{l_m}}_{\text{shift}}) \tag{6}$$

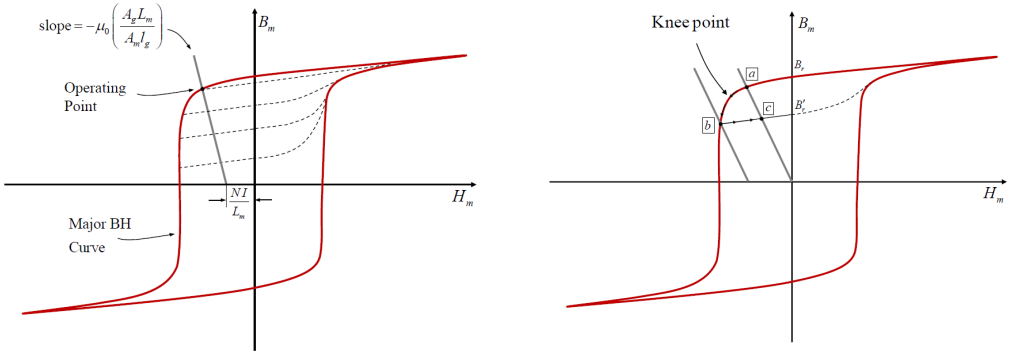

(a) Operating point can be changed by shifting the load line through an applied current to the coil [4].

(b) The PM is demagnetized from point a to b. When the current is removed, the operating point follows the recoil line to a new remanent state c [4].

Figure 4. A visual representation of Magnetization state tuning in the B-H domain

B. Magnet demagnetization

Figure 4(b) highlights the knee-point of the Major loop hysteresis curve. Suppose that the magnet's operating point is in point[a]. When sufficient current I_{tune} is supplied to the curve, the load line and operation point shift past the knee-point towards point [b] the so-called corner-point. When the desired corner point is reached, The input voltage is removed and the current decays to 0A, the operation point then follows a recoil line because the major loop curve can only be traversed anti-clockwise. Operation point [c] is now the new rest state. Consequently, the flux in the actuator and thus the force output has reduced. The energy input required for this operation can be calculated by:

$$E_{\text{hyst}} = A_m l_m \int H_m dB \tag{7}$$

which can be visualized by the area that is encircled in the B-H curve during the tuning process, and:

$$E_{TM,\,\text{copper}} = \int_0^T I_{tune}^2(t) R dt \tag{8}$$

Which are the resistive losses in the tuning coil with tuning time T and tuning coil resistance R. It is important to note that traversing the BH curve is time and history-dependent and therefore the recoil lines are different when entered from the left or from the right side of the Major loop [6]. Different algorithms are available to tune the magnet. They are described in the preliminary knowledge section.

C. Hybrid Tunable Magnet actuator

Permanent NdFeB magnets can be used to generate bias fluxes in the circuit to create a linear force-flux relation which improves the accuracy of the actuator when a linear controller is used. Figure 5a shows an example of such a Hybrid Reluctance Actuator (HRA). The bias flux in the left gap adds to ϕ_{drive} and the bias flux in the right gap gets subtracted. The Maxwell stress tensor for this actuator (eq. 9), shows that the force-flux relation can be reduced to linear eq. 10.

$$F = \frac{\left(\phi_{pm,gapL} + \phi_c\right)^2 - \left(\phi_{pm,gapR} - \phi_{drive}\right)^2}{2\mu_0 A_g} \tag{9}$$

$$\begin{aligned} F &= \frac{\phi_{pm}}{\mu_0 A_g}\left(\phi_{drive} + \phi_{pm}\frac{x}{2l_g}\right) \\ F &= K_{drive} I_{drive} + k_a x \end{aligned} \tag{10}$$

W. Hoekwater [8] drew inspiration from this to design a TMA with a linear force flux relation. Figure 5b shows his design. Note that the coercivity of the NdFeB magnets is much higher and is therefore not significantly influenced by external fluxes. The layout of the NdFeB magnets are important to the concept Because the flux of the TM (red) should not be shortcutted by iron yokes. If it is shortcutted, no flux will flow through the mover and thereby no force will be generated. Both PM's act as a barrier for the TM flux as well as providing the bias flux similar to the HRA concept. Because the reluctance of a permanent magnet is very high, it is inefficient to have the flux from the TM pass through the PM's, therefore the two separate flux loops are created. The Maxwell stress tensor again shows the linearity of the actuator with respect to the flux in the TM in eq. 12

$$F = \frac{\left(\phi_{pm,gL} + \phi_{tm}\right)^2 - \left(\phi_{pm,gR} - \phi_{tm}\right)^2}{2\mu_0 A_g} \tag{11}$$

$$\begin{aligned} F &= \frac{2\phi_{pm}}{\mu_0 A_g}\left(\phi_{tm} + \phi_{pm}\frac{2x}{2l_g + \mu_0 A_g \mathcal{R}_{tm}}\right) \\ F &= K_{tm} B_{tm} + k_a x \end{aligned} \tag{12}$$

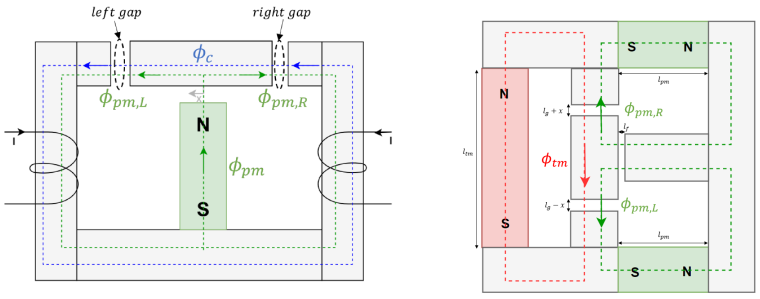

(a) A Hybrid Reluctance Actuator design (HRA) [8]

(b) A Hybrid Tunable Magnet Actuator design (HTMA) [8]

Figure 5. Hybrid variants with NdFeB magnets in green and the Tunable AlNiCo5 magnet in red.

III. Design of a Dynamic Tunable Magnet Actuator

A. Concept Design

The challenge in electromagnetic actuation is to reduce heat dissipation. The development of tunable magnet actuation is a solution to counter this, providing a constant force without constant heat dissipation. However, the energy input required to (de)magnetize the magnet, still results in heat dissipation. Therefore, it's only efficient if the TMA operates quasi-statically.

This research proposes a Tunable Magnet Actuator design that has two controllable sources of magnetic fields. First the AlNiCo5 magnet for steady state forces with corresponding tuning coil to change its remanent state and a drive coil like it would be used in a conventional reluctance actuator for dynamic actuation. Therefore the actuator will be referred to as the Dynamic Hybrid Tunable Magnet acuator.

In order to have an efficient actuator, the motor constant must be maximized. With this in mind, the following design principles should be applied:

1) Both the tunable magnet flux and drive flux paths should not be able to shortcut the mover. No flux in the air gaps means no force is exerted on the mover.
2) Permanent magnets with a high coercivity (NdFeB) can provide bias flux ϕ_{pm} to increase the linearity and motor constant of the actuator
3) The drive flux path ϕ_{drive} should not pass through the TM. This is because of two reasons. Firstly, the TM itself has a high reluctance and thus acts as a large air gap, reducing the motor constant. Secondly, the drive flux could affect the magnetization state of the TM unintentionally.
4) The tunable magnet flux ϕ_{tm} and the drive flux path ϕ_{drive} should not pass through the permanent magnets. The PMs also act as an air gap and this increases the reluctance, reducing the motor constant.

Note that the HRA and the HTMA from fig. 5a and 5b could be connected in parallel by rigidly connecting their movers with a non-ferromagnetic material as proposed by [7], which is reviewed in Appendix D. The two actuators keep their own characteristics and fulfill the design principles mentioned above.

However, this research proposes a design that combines the two actuators into a single magnetic circuit as shown in fig. 6. The top part resembles the HRA design from fig. 5a with two drive coils connected in series providing a variable force with its flux path shown in blue and PM A to provide a bias flux. The bottom part resembles the HTMA in fig. 5b as designed by [8] with the tunable magnet flux path shown in red and the PM's B and C in the center-right and -left, providing a bias flux. This is a more efficient design than the parallel connected HRA $ HTMA layout because, for the same amount of material, the motor constant for the drive side is doubled while maintaining the performance of the tunable magnet.

B. Design analysis

The increased motor constant can be explained by the fact that the permanent magnets B and C now also contribute to the motor constant, whereas in the parallel setup, the flux paths were completely separated. Because PMs B and C also provide a bias flux for the drive coil flux, PM A is not necessary for this concept to function as intended, but the extra bias flux it provides, adds to the motor constant of the drive side. A downside of having PM A is that it adds to the negative stiffness that could complicate controlling the actuator, this is a feature that most hybrid actuators suffer from. Their negative stiffness creates an unstable system. To account for this, positive stiffness needs to be added either mechanically or virtually by controlling the drive coil. In this actuator, the bias fluxes in the top and bottom are uneven, and thus the bias flux generated by PM A contributes to a moment generated in the mover. In general, moments exerted on the mover is a potential issue with this design, because the forces in the upper and lower gap are designed to be independent. Linear guidance should aim to prevent the rotation of the mover.

PM B and C do not only provide bias flux but also act as large air gaps to separate tunable magnet and drive coil flux paths. Shorter magnets would increase the force density as the reluctance of their flux paths would decrease but a certain length is required to limit the influence the drive coil has on the tunable magnet and prevent mixing of the controllable flux paths ϕ_{drive} and ϕ_{tm}. Geometries of all components could be optimized for the best force density but that is beyond the scope of this research. Further design considerations and alternative designs can be found in Appendix A.

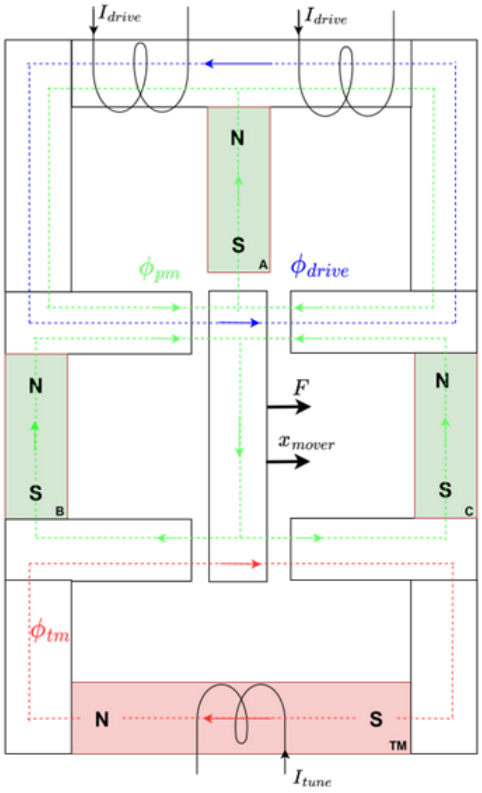

Figure 6. The schematic design of the Dynamic Hybrid Tunable Magnet Actuator

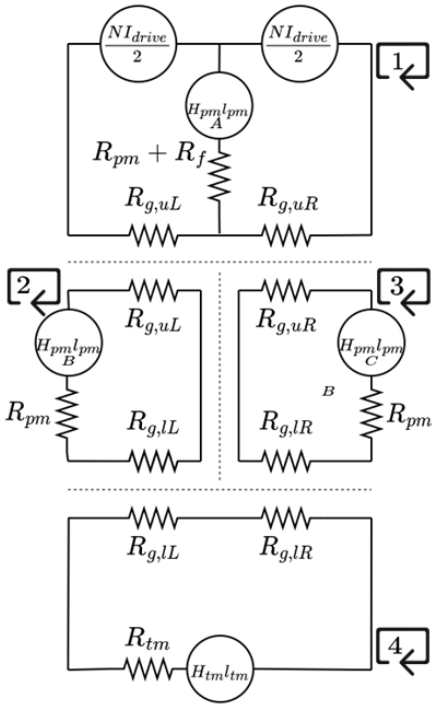

Figure 7. Magnetic Equivalent Circuit model with superposition of the different flux loops

C. Actuator characteristics

In order to model the new actuator design, the Maxwell stress tensor in eq. 13 relates the fluxes in the air gaps to the force on the mover. Using the Magnetic Equivalent Circuit method and the principle of superposition, the six unknown fluxes can be found. The first two are the drive coil flux ϕ_{drive} in the upper gaps and TM flux ϕ_{tm} in the lower gaps which can be adjusted independently by the controller of the actuator. The permanent magnets provide the bias fluxes from the permanent magnets in the left and right, upper and lower air gaps, $\phi_{pm,g,uL}$,$\phi_{pm,g,uR}$,$\phi_{pm,g,lL}$, and $\phi_{pm,g,lR}$. These fluxes only vary with the position of the mover.

$$F = \frac{\left(\phi_{pm,g,uL}+\phi_{drive}\right)^2-\left(\phi_{pm,g,uR}-\phi_{drive}\right)^2}{2\mu_0 A_g} + \frac{\left(\phi_{pm,g,lL}+\phi_{tm}\right)^2-\left(\phi_{pm,g,lR}-\phi_{tm}\right)^2}{2\mu_0 A_g} \tag{13}$$

The Magnetic Equivalent Circuit method models magnetic circuits as electronic circuits. Figure 7 shows how the actuator can be modeled as a set of voltage sources and resistors that induce a current, which are a representation of the MMF sources, air gaps, and magnetic flux respectively. It is important to note that this is a simplification and that unlike in electronic circuits, isolation of magnetic fields is very difficult. However, to better understand the concept and flux paths, the circuit is considered to be ideal. That means that no flux losses are present and that the yokes have negligible reluctance. The reluctances of the air gaps are dependent on the position of the mover x. The gap length when the mover is in the mid position is l_g and the fixed air gap between the mover and PM A has length l_f. Together with the magnet reluctances, they can be expressed as:

$$
\begin{aligned}
R_{g,uL} &= \frac{lg+x}{\mu_0 A_g}, R_{g,uR} = \frac{lg-x}{\mu_0 A_g} \\
R_{g,lL} &= \frac{lg+x}{\mu_0 A_g}, R_{g,lR} = \frac{lg-x}{\mu_0 A_g} \\
R_{pm} &= \frac{l_{pm}}{\mu_0 A_{pm}}, R_{tm} = \frac{l_{tm}}{\mu_0 \mu_r A_{tm}} \\
R_f &= \frac{l_f}{\mu_0 A_{pm}}
\end{aligned} \tag{14}
$$

Using Hopkinson's law, the flux in the four separate loops in fig. 7 can be approximated assuming an ideal circuit by $\phi = \frac{MMF}{R}$.

1) Loop 1, The flux from the drive coil:

$$
\phi_{drive} = \frac{NI_{drive}}{R_{g,uL} + R_{g,uR}} \tag{15}
$$

The flux from PM A

$$
\phi_{pm,A} = \frac{H_{pm} l_{pm}}{R_{g,uL} + R_{g,uR} + R_{pm}} \tag{16}
$$

2) Loop 2 The flux from PM B

$$
\phi_{pm,B} = \frac{H_{pm} l_{pm}}{R_{g,uL} + R_{g,lL} + R_{pm}} \tag{17}
$$

3) Loop 3, The flux from PM C

$$
\phi_{pm,C} = \frac{H_{pm} l_{pm}}{R_{g,uR} + R_{g,lR} + R_{pm}} \tag{18}
$$

4) Loop 4, The flux from the Tunable Magnet

$$
\phi_{tm} = \frac{H_{tm} l_{tm}}{R_{g,lL} + R_{g,lR} + R_{tm}} \tag{19}
$$

With all loop fluxes known, the superposition principle is applied to find the bias fluxes in the four air gaps from the permanent magnets:

$$
\begin{aligned}
\phi_{pm,g,uL} &= \frac{l_g+x}{2l_g}\phi_{pm,A} + \phi_{pm,B} \\
\phi_{pm,g,uR} &= \frac{l_g-x}{2l_g}\phi_{pm,A} + \phi_{pm,C} \\
\phi_{pm,g,lL} &= \phi_{pm,B} \\
\phi_{pm,g,lR} &= \phi_{pm,C}
\end{aligned} \tag{20}
$$

With the results of eq. 15, 19 and 20, the Maxwell stress tensor from eq. 13 can be evaluated to the following:

$$
\begin{aligned}
F \approx \frac{\phi_{pm,g,u}}{\mu_0 A_g}\left(\phi_{drive} + \phi_{pm,g,u}\frac{x}{2l_g}\right) + \\
\frac{2\phi_{pm,g,l}}{\mu_0 A_g}\left(\phi_{tm} + \phi_{pm,g,l}\frac{2x}{2l_g + \mu_0 A_g R_{tm}}\right)
\end{aligned} \tag{21}
$$

Equation 21 can be simplified to a linear equation where K_{drive} and K_{tm} represent the motor constants and k_a the actuator stiffness:

$$
F = K_{drive}\mathbf{I_{drive}} + K_{tm}\mathbf{B_{tm}} + k_a\mathbf{x} \tag{22}
$$

Figure 8 shows the force-current relation of the new design. K_{drive} represents the slope and the force-flux relation for the tunable magnet $K_{tm}B_{tm}$ can be visualized by the motor characteristic shifting up and down, changing the output force range, while maintaining a low input current.

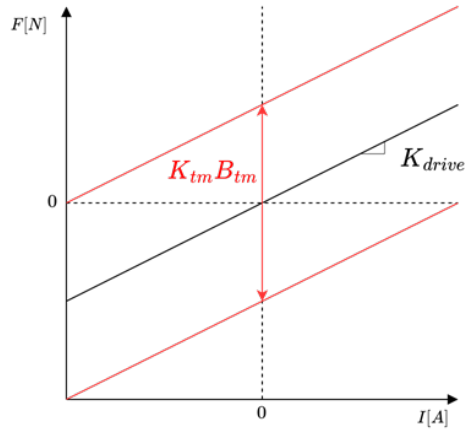

Figure 8. Actuator Characteristics of the Dynamic Hybrid Tunable Magnet Actuator at x=0

IV. Detailed design analysis

To validate the concept and further study its characteristics, a prototype actuator is designed. A 3D FEM model is then analyzed in COMSOL Multiphysics to predict the performance and better understand magnetic non-idealities in the system.

In order to benefit from prior research by [4], [8], and [7], the tunable magnet and tuning coil is kept the same as in their work. For this magnet, the material properties, tuning algorithms, and characteristics are known and therefore, this is a starting point for the design requirements. To validate the energy dissipation benefit of this actuator, both the drive coil and the tunable magnet sides should be able to deliver a similar output force with the available lab equipment and materials. These basic requirements are listed in table 1.

Table 1. Actuator design Targets

Symbol	Value	Comment
$F_{tm,max}$	$\pm 10N$	TM Force range, set by prior work [8]
$F_{drive,max}$	$\pm 10N$	drive coil force range, to compare to TM
$I_{drive,max}$	$\pm 5A$	Max current input with available hardware
x_{max}	$\pm 0.5mm$	movement range with available flexures
l_g	$> 1mm$	min required gap length to fit Hall sensors

Table 2. Actuator Design Parameters

Symbol	Value	Comment
AlNiCo 5 magnet		
l_{tm}	$30mm$	Tunable Magnet length
d_{tm}	$10mm$	Tunable Magnet diameter
$B_{r,tm}$	$1.25T$	remanent flux density
$H_{c,tm}$	$50kAm^{-1}$	coercive force
$\mu_{r,tm}$	$0.95B_{r,tm} + 4.96$	relative permeability recoil lines
NdFeBr magnet		
l_{pm}	$20mm$	magnet length
w_{pm}	$10mm$	magnet width and height
B_{rpm}	$1.38T$	remanent flux density
$\mu_{r,pm}$	1.05	relative permeability
Magnetic circuit		
$\mu_{r,es}$	4000	relative permeability
A_g	$10x15mm$	air gap surface area
l_g	$1.25mm$	length air gap in mid position
l_f	$1mm$	length fixed air gap
N_{coil}	200	total # of drive coil windings

With manufacturability and availability of components in mind, the conceptual schematic layout from fig. 6 is developed into a CAD model shown in fig. 9. The dimensions and material properties can be found in table 2.

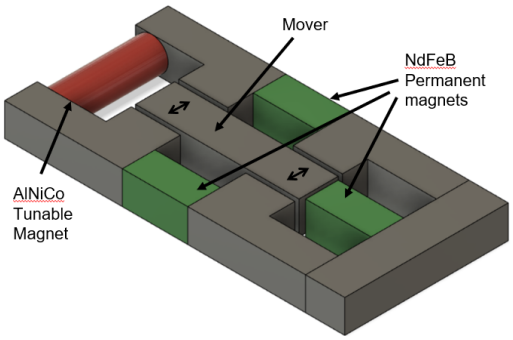

Figure 9. A CAD design of the Dynamic HTMA

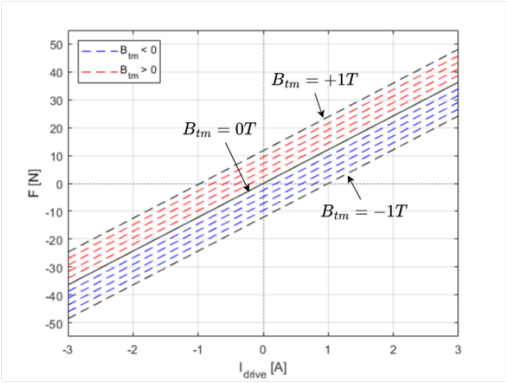

Figure 10. FEA result of the actuator characteristics at $x = 0mm$.

A. Actuator Characteristics

Figure 10 shows the actuator characteristics when the mover is in the mid position. The slope of the line represents the motor constant, K_{drive}, and the shift up and down is due to the magnetization state tuning, $K_{tm}B_{tm}$. The Actuator has a negative stiffness which contributes to the output force if the mover is not in the middle position. Table 3 summarizes the actuator characteristics as specified in eq. 22. For simplicity, the motor constants are reduced to a linear model around the actuator rest state and mid-position. i.e. $I_{drive} = 0A$, $B_{tm} = 0T$, and $x_{mover} = 0mm$. Non-linear effects like flux losses and fringing fluxes that occur with mover displacement are discussed in the next section.

Table 3. Actuator characteristics found by COMSOL FEA

Symbol	Value	Comment
K_{drive}	$12.4N/A$	Motor constant
K_{tm}	$12.2N/T$	Motor constant
K_a	$-59.4kN/m$	Actuator stiffness
x_{max}	$\pm 0.2mm$	movement range
$F_{max,x=0}$	$\pm 48.6N$	Combined Force range

B. Modeling non-idealities

To accurately tune the magnet, the magnet operating point must be known, for this, the load line is used.

$$B_m = -\mu_0 \frac{A_g l_m}{2A_m l_g(x)} (H_m - \frac{NI_{tune}}{l_m}) \tag{23}$$

Equation 23 was derived using a lumped parameter model with an ideal magnetic circuit. In reality, fringing and leakage fluxes and MMF loss due to material properties occur in the system. To account for this in the load line equation, correction factors should be applied. Because the variable air gaps play a significant role in losses, the correction factors are defined as a function of the mover position. Using the COMSOL Multiphysics FEA model, the loss factors can be found and described by a polynomial fit. In this design, 4 correction factors are applied:

1) The flux loss in TM circuit changes the slope of the load line, indicated by k_L and k_R.

$$k_L = \frac{\phi_{tm,gL}}{\phi_{tm}}, k_R = \frac{\phi_{tm,gR}}{\phi_{tm}} \tag{24}$$

2) The magnetomotive force loss in TM circuit that changes the slope of the load line, indicated by k_{MMF}.

$$k_{MMF} = \frac{H_L \left(l_g - x\right) + H_R \left(l_g + x\right)}{H_{tm} l_{tm}} \tag{25}$$

3) The applied magnetic field on the TM by all NdFeB magnets in the circuit that shifts the load line, indicated by k_{pm}.

$$k_{pm} = \frac{MMF_{pm's@tm}}{MMF_{1pm}} \tag{26}$$

4) The applied magnetic field on the TM by the drive coil that shifts the load line, indicated by k_x where:

$$k_x = \frac{MMF_{drive@tm}}{MMF_{drive@coil}} \tag{27}$$

With these corrections applied to the load line, the equation is expanded to the following:

$$B_{tm} = c\left(H_{tm} - \frac{NI_{tune}}{l_{tm}} - k_{pm}\frac{MMF_{1pm}}{l_{tm}} - k_x\frac{NI_{drive}}{l_{tm}}\right) \tag{28}$$

where:

$$c = -\frac{k_{MMF}\mu_0 A_g l_{tm}}{\left(\left(k_L + k_R\right) l_g + \left(k_R - k_L\right) x\right) A_{tm}} \tag{29}$$

Table 4. Loss correction factors found in FEA

Mechanism	Symbol	Polynomial fit
Flux loss Left	k_L	$0.07x^2 + 0.13x + 0.34$
Flux loss Right	k_R	$0.07x^2 - 0.13x + 0.34$
MMF loss	k_{MMF}	$-3.4 \cdot 10^{-3}x^2 - 1.98 \cdot 10^{-4}x + 0.984$
PM influence on TM	k_{pm}	$0.22x - 1.6 \cdot 10^{-3}$
Cross act. influence	k_x	$7.6 \cdot 10^{-5}x^2 + 1 \cdot 10^{-7}x - 1.2 \cdot 10^{-4}$

Table 4 shows the results of the FEA. The flux loss factors show that only $\sim$ 34% of the tunable magnet flux contributes to the force output. This is mainly due to the high reluctance of the tunable magnet flux path. If the length of the tunable magnet would be reduced, k_L/k_R and consequently K_{tm} would increase. The influence of the magnetomotive force loss is low due to the high permeability of the electrical steel. The influence of the PM's magnetic fields on the TM can affect the magnet tuning. k_{PM} can shift the load line up to 2% of $H_{c,tm}$ when moved to the extreme positions. With the slope of the major B-H curve in mind, this can lead to tuning errors of up to $0.34T$. Finally, the shift in load line due to the magnetic field of the drive coil is negligible at a maximum of $\approx 2.4A/m$ at $I_{drive} = 3A$ and $x = 0.2mm$. This is attributed to the length of PM B and C as discussed in section III. It is expected that if those magnets are replaced with shorter variants, k_x will increase.

C. Actuator performance

To show the benefit of using the Dynamic HTMA, the energy dissipation of the novel actuator design is compared to a hypothetical Hybrid Reluctance Actuator without a tunable magnet but with the same motor constant K_{drive}. Based on the actuator characteristics from table 3, the heat dissipation for different reference signals is calculated by eq. 30

$$P = I_{drive}^2 R \tag{30}$$

The reference force signal has a dynamic component that is a sinusoid with an Amplitude of $F_A = 1N$, a frequency of $f = 3Hz$, and a constant offset component F_0 of $0N$,$2.5N$ and $5N$.

$$F_{ref} = F_A sin(2\pi f t) + F_0 \tag{31}$$

In the new design, the controller should be designed to separate both terms and use the drive coil for the sinusoidal term and the TM for F_0. The reluctance actuator with the same motor constant will have to deliver more current to also provide constant magnetic flux for the F_0 term. For the Dynamic HTMA, a worst-case energy dissipation of $0.3J$ is used for tuning the magnet to provide the required F_0. The results are shown in fig. 11.

For $F_0 = 0$, both actuators work identically as only the drive coil is actuated and both actuators have an identical K_{drive}. When F_0 is increased, the HRA shows exponentially more energy dissipation. The Dynamic HTMA requires an initial energy input of $E_{tune} = 0.3J$ but I_{drive} only needs to deliver the dynamic part of the signal. Therefore, the

actuator is increasingly more efficient for larger values of F_0. E_{tune} not only depends on the targeted tuning state but also the previous state due to the hysteresis inside the AlNiCo 5 magnet. Because the tuning energy becomes less significant with larger force offsets, the efficiency bandwidth of the TM increases.

From a different perspective, the force range for the same continuous energy dissipation is increased when a TM is used. Suppose a continuous heat dissipation as a result of $I_{drive} = 1A$ is acceptable for a system. The HRA then allows a force range of $\pm 12.4N$. While the TM brings allows a force range of $\pm 24.6N$ for the same energy dissipation. This is visualized in fig. 12 which shows the force range of the HRA in red and the expanded force range in green.

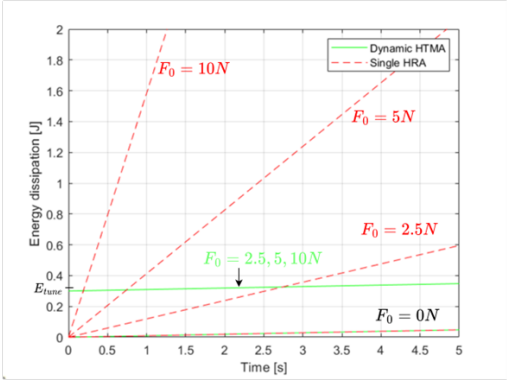

Figure 11. The energy dissipation over time of both actuators following the reference signal with $F_0 = 0, 2.5, 5$ and $10N$.

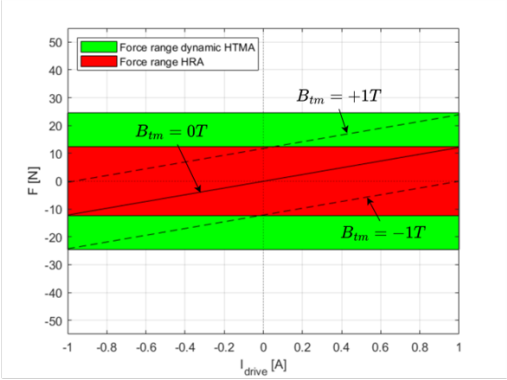

Figure 12. The Dynamic HTMA has an increased force range for equal energy input.

V. Conclusion

A. Conclusion

To deal with the efficient frequency bandwidth limitation of the TMA, this work explored the working principle of combining a Tunable Magnet actuator and a Reluctance Actuator. A design that uses a tunable magnet actuation for quasi-steady state outputs and a drive coil for higher frequency actuation is proposed and analyzed. The main contribution to the state-of-the-art in Tunable magnet technology can be summarized by the following points:

- The Dynamic Hybrid Tunable Magnet Actuator now allows for tracking of high-frequency signals. This is due to the additional functionality of the drive coil. It shows the benefit of implementing TM technology into existing Actuator applications. Furthermore, the drive coil can also compensate for inaccuracies or transient states of the TM.
- Heat dissipation is significantly reduced if a signal is offset. This is due to the separation of low and high-frequency signals reducing the work the drive coil has to deliver.
- The TM increases the maximum force range of a reluctance actuator for the same heat dissipation. This was visualized by shifting the motor constant up and down. Using the TM, the position or force output at the resting state ($I_{drive} = 0A$) can be changed as desired.

With these 3 points in mind, the actuator would be suited for an application such as a gravity compensator that requires high-frequency bandwidth to reject disturbances and a steady state force to support the weight of an object. The drive current and tunable magnet inputs can be linearly related to force output allowing for a linear controller. Using COMSOL Multiphysics for a magnetic Finite element analysis on a more detailed design, the motor constants are found at $12.4N/A$ for the drive coil and $12.2N/T$ for the Tunable magnet. With these parameters, the heat dissipation in the system is compared to a single reluctance actuator. Although there is an initial energy penalty of up to $0.3J$ for tuning the magnet, the continuous energy dissipation after tuning is reduced by $\sim 98\%$ for a sinusoidal dynamic signal with a steady-state offset of $5N$.

B. recommendations

For future work, the following recommendations are made:

- An experimental setup was designed which is shown in Appendix B. This is useful to verify the FEA results, use as a test bed for a controller design, and verify the dynamic behavior.
- There is a big challenge in the control aspect. The drive coil can be used to compensate for mover disturbances from tuning the magnet as there is an inherent overshoot due to the required flux from the tuning coil to change the magnetization state of the TM. Furthermore, a control algorithm needs to determine whether the actuator should use the drive coil or the TM to follow a reference signal. It may be unknown if a disturbance is short, like external floor vibrations, or can be a quasi-steady state like drift or temperature offsets.
- The 2D schematic approach easily shows the flux paths, but the long magnets are not efficient due to their high reluctance. The geometry of all components can be optimized for motor constant and force density. Shorter magnets, a 3D design yoke with flux losses in mind, and small air gaps can prove beneficial to reduce heat dissipation. Using this actuator concept for an application like the gravity compensator will give clear requirements and can optimize the design to meet the performance targets.

References

[1] M, S. R., G, S., A, R., and van Eijk J, *The Design of High Performance Mechatronics*, 3rd ed., IOS Press, 2020.

[2] Knaian, A., "Electropermanent magnetic connectors and actuators : devices and their application in programmable matter," 2010, p. 208. URL http://dspace.mit.edu/handle/1721.1/60151.

[3] Hüfner, T., Radler, O., Ströhla, T., Sattel, T., Wesselingh, J., Vogler, A., and Eicher, D., "A note on electromagnetic gravity compensation actuators based on soft electro-permanent magnets for adjustable reluctance force," *Proceedings of the 17th International Conference of the European Society for Precision Engineering and Nanotechnology, EUSPEN 2017*, 2017, pp. 149–150.

[4] Viëtor, S., "Tunable Magnets: Modeling and Validation for Dynamic and Precision Applications," *Thesis Topology*, 2018, pp. 5–7.

[5] Meijer, R., "Modeling and prototyping of a Tuneable Magnet actuator for quasi-static and low-frequency dynamic applications," 2020, pp. 1–25.

[6] Wiersema, J. D., "Tunable Magnet Actuators: Hysteresis Modelling for Efficient and Accurate Magnetization State Tuning," , 2022. URL http://repository.tudelft.nl/.

[7] Ronaes, E. P., "Tunable Magnet Actuators: Remnant Magnetisation State and Position Control of a Hybrid Tunable Magnet Actuator," , 2023.

[8] Hoekwater, W. B., Ronaes, E., and HosseinNia, H., "Hybrid Tunable Magnet Actuator: Design of a Linearized Force-Flux Tunable Magnet Actuator," *IEEE Transactions on Industrial Electronics*, 2023, pp. 1–10. doi: 10.1109/TIE.2023.3285984.

[9] Furlani, E. P., *Permanent magnet and electromechanical devices*, Vol. 148, ????

4. Conclusion and Recommendations

4.1. Conclusion

Tunable Magnet Actuation is a solution to the problem of heat dissipation in electromagnetic actuation. However, its application is limited to quasi-steady state actuation only. To deal with this limitation, the following goal was set:

Develop a Hybrid Tunable Magnet Actuator that is capable of high-frequency actuation with low heat dissipation.

This work explored the working principle of combining an efficient tunable magnet for quasi-steady state outputs and a drive coil for higher frequency actuation to achieve efficient actuation at a higher frequency range. The conclusions are discussed below using the objectives set at the beginning of the project.

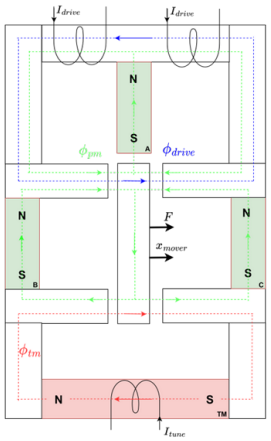

Figure 4.1: Dynamic Tunable Magnet Actuator

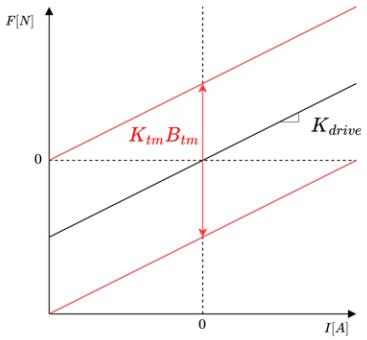

Figure 4.2: Actuator Characteristics of a combined Hybrid Tunable magnet actuator at x=0

1. **Develop a concept that combines a tunable magnet and a drive coil that maximizes the motor constants to minimize heat dissipation.** This research proposes a design that combines two existing actuator designs into a single magnetic circuit as shown in figure 4.1. The top part resembles the HRA with two drive coils connected in series providing a variable force with its flux path shown in blue and PM A to provide a bias flux. The bottom part resembles the HTMA as designed by [1] with the tunable magnet flux path shown in red and the PM's B and C in the center-right and -left, providing a bias flux.

2. **Model the actuator with a 1st-order model to prove the functionality and illustrate the actuator characteristics.** Using a lumped parameter model and superposition to find the fluxes present in the air gaps. The Maxwell stress tensor can be evaluated and simplified to a linear equation where K_{drive}, K_{tm} represent the motor constants and k_a the actuator stiffness:

$$F = K_{drive}\mathbf{I_{drive}} + K_{tm}\mathbf{B_{tm}} + k_a\mathbf{x} \tag{4.1}$$

Figure 4.2 shows the force-current relation of the new design. K_{drive} represents the slope and the force-flux relation for the tunable magnet $K_{tm}B_{tm}$ can be visualized by the motor characteristic shifting up and down, changing the output force range, while maintaining a low input

current.

3. **Develop more detailed 3D model that can be analyzed with a finite element model to provide the motor constants, study non-idealities that can affect the operation of the actuator, and prove the benefit of this actuator compared to a conventional reluctance actuator that has a similar motor constant.**
   Using COMSOL Multiphysics for a magnetic Finite Element Analysis on a more detailed design, the motor constants are found at $12.4 N/A$ for the drive coil and $12.2 N/T$ for the Tunable magnet. 4 correction factors are used to account for non-idealities during the magnet tuning. These are applied to the load line. Most noticeable is the 66% loss in flux between the TM and the air gaps due to the sub-optimal dimensions of the TM and the influence the permanent magnets can have on the TM tuning when the mover is not in the middle position.
   With these parameters, the heat dissipation in the system is compared to a hypothetical single reluctance actuator. Although there is an initial energy penalty of up to $0.3 J$ for tuning the magnet in the dynamic HTMA, the continuous energy dissipation after tuning is reduced by $\sim 98\%$ for a sinusoidal dynamic signal with a steady-state offset of $5N$, which is in line with the initial estimations made before the start of the project as shown in Appendix C.

4. **Develop a simple control algorithm and build a test setup to verify the FEA results and validate the concept.** Unfortunately, due to time constraints, it was not possible to build a test setup to execute an experiment in this thesis project. However, practical designs were made and some components were fabricated. Appendix B shows the plans for this setup for future students working on this project.

The main contribution to the state-of-the-art in Tunable magnet technology can be summarized by the following points:

- The Dynamic Hybrid Tunable Magnet Actuator now allows for tracking of high-frequency signals. This is due to the additional functionality of the drive coil. It shows the benefit of implementing TM technology into existing Actuator applications. Furthermore, the drive coil can also compensate for inaccuracies or transient states of the TM.
- Heat dissipation is significantly reduced if a signal is offset. This is due to the separation of low and high-frequency signals reducing the work the drive coil has to deliver.
- The TM increases the maximum force range of a reluctance actuator for the same heat dissipation. This was visualized by shifting the motor constant up and down. Using the TM, the position or force output at the resting state ($I_{drive} = 0A$) can be changed as desired.

This would make it very suited for Gravity compensation applications. The high-frequency actuation can reject floor vibrations and isolate the end effector while not having to provide force counteracting the gravity of the object itself. If the mass of the end-effector changes, the magnet tuning can be used to provide a different gravitational force. This is similar to the magnetic gravity compensator of [10] in figure D.2. However, in the dynamic HTMA, there are no moving components that require lubrication or wear out.

4.2. Recommendations

For future work, the following recommendations are made:

- **Complete the experimental setup of the dynamic HTMA** An experimental setup was designed which is shown in Appendix B. Completing this setup can verify the FEA results and show any practical implications. If it works as expected, it can be used as a test bed for a controller design

(see next point), and to verify the dynamic behavior.

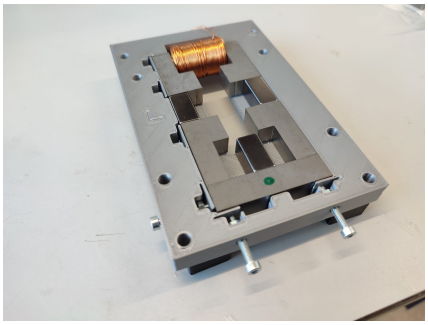

(a) Dynamic HTMA without the mover in place.

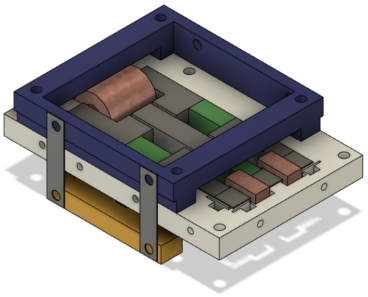

(b) The CAD design of the Dynamic Hybrid Tunable Magnet actuator with support structure and flexures.

Figure 4.3: The intended Experimental setup of the Dynamic HTMA

- **Design a controller to separate low and high-frequency actuation** In this research, it is shown that the concept of separating the low- and high-frequency signals can provide a significant reduction in heat dissipation. However, this is not possible without an algorithm to control this separation. A control algorithm needs to determine whether the actuator should use the drive coil or the TM to follow a reference signal. It may be unknown if a disturbance is short, like external floor vibrations, or can be a quasi-steady state like drift or temperature offsets. a controller design previously suggested by [7] is shown in figure 4.4

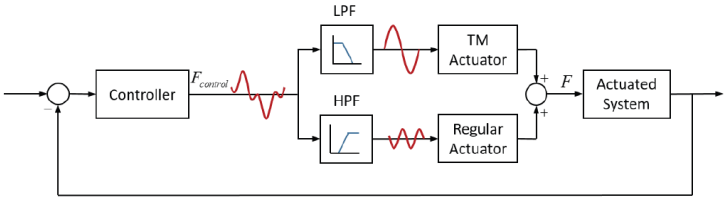

Figure 4.4: A closed loop controller with a parallel combination of TM actuator and 'regular' actuator [7]

Furthermore, The drive coil can be used to compensate for mover disturbances from tuning the magnet as there is an inherent overshoot due to the required flux from the tuning coil to change the magnetization state of the TM.

- **Optimize the geometry of all magnets and yokes for a high motor constant** The 2D schematic approach easily shows the flux paths, but the long magnets are not efficient due to their high reluctance. The geometry of all components can be optimized for motor constant and force density. Shorter magnets, a 3D design yoke with flux losses in mind, and small air gaps can prove beneficial for reducing the flux losses.

A. Design Considerations

A.1. Series versus Parallel

Combined actuators are used in systems where the use of a single actuator would be unsuitable or inefficient. Combined actuators exist in various forms. A distinction can be made between how the force is exerted on the end-effector, either parallel or in series as illustrated in figure A.1

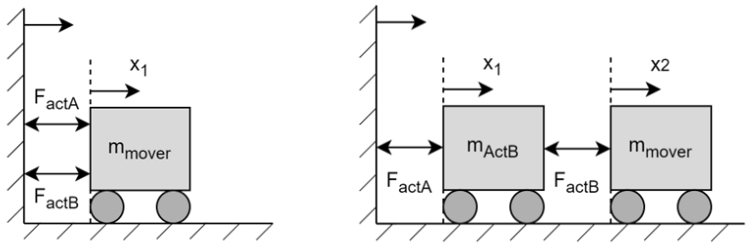

(a) Two actuators (A and B) act on the same end effector/mover, the forces can be combined as a resultant force.

(b) he actuators A and B are separate in this case and actuator b is part of the mover of actuator A.

Figure A.1: Parallel vs Combined actuation

The series arrangement is very common in positioning stages where one actuator has a large position bandwidth (coarse stage) and the other a small position and force bandwidth (fine stage). A good example of this is A Hard-Disk drive where a Lorentz actuator controls the large movements in the reading arm and a piezo at the end of the arm provides position compensation.
The parallel arrangement is much less common. Suppose one of the actuators has a high stiffness like a piezo actuator. In that case, the Force of the other actuator on the mover is used to stretch the other actuator, and thus it only efficient when both actuators are providing the same force. For low-stiffness actuators (most electromagnetic actuators), this is less of an issue. The two separate forces act on the same 1DOF body and can be added and subtracted to a single resultant force. Although there could be some undesired redundancy or they can work against each other, it does provide the opportunity to use 2 separate actuators that operate on different force or frequency levels.

If the Combined TMA and HRA actuator would be split and set up in a series layout. The dynamics involved are complicated due to the comparable mass and stiffness of both actuators. Any force provided by one actuator is likely to affect the other actuator's position too.
For the HDD example, the piezo-actuator is relatively light and has a position bandwidth that is of a much lower order of magnitude. Therefore movements made by the piezo are much less influential on the Lorentz actuator.
To keep the system dynamics as simple as possible, it is preferred to use the parallel type layout in the combined actuator design.

A.2. Actuator Concept Evaluation

This section discusses a range of conceptual layout options that fit the chosen strategy of a Parallel actuator. Any further mention of a 'concept' refers to the way the magnets and coils are placed and connected with yokes to provide flux paths to the mover. The main functionality requirements are:

- Both the TM and drive coil parts are able to deliver a force independently
- The forces from the TM and drive coil act on the same mover and can therefore be added up
- In the rest state the actuator should be able to deliver 0N. Uncarefully placed PM's can change this.

The Wishes are

- High motor constants $F = K_{drive}\mathbf{I_{drive}} + K_{tm}\mathbf{B_{tm}} + k_a\mathbf{x}$
- Good force-flux Linearity
- A bi-directional force
- Minimal complexity
- Compactness

W. Hoekwater set out to design a combined actuator too before he shifted his attention to designing the hybrid tunable magnet actuator. His suggested designs are shown in figure A.2. Each design is marked with a X, O, or checkmark to state if it fulfills the requirement as mentioned above. X means, not at all, O means with little adjustment and a checkmark means it is okay with the requirements. The Double RA Double C-TMA and Double RA Double E-TMA are very similar and are therefore considered as the same concept.

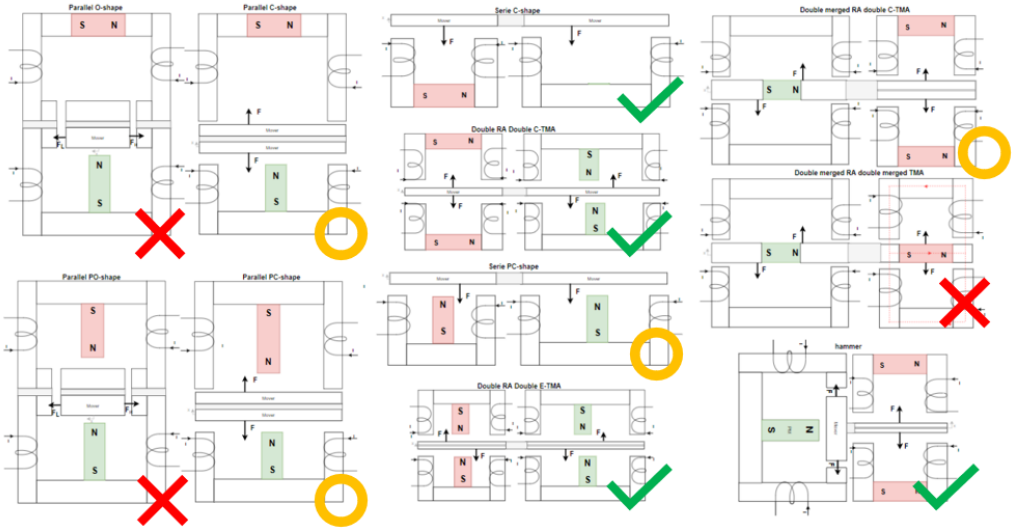

Figure A.2: Conceptual designs proposed by W. Hoekwater [1]

The parallel HRA & HTMA as designed by E. Ronaes [2], also fits the requirements. Finally, the novel design that integrates the HRA and HTMA design into a single magnetic circuit is considered. The collection of actuator concepts that are evaluated are shown in figure A.3.

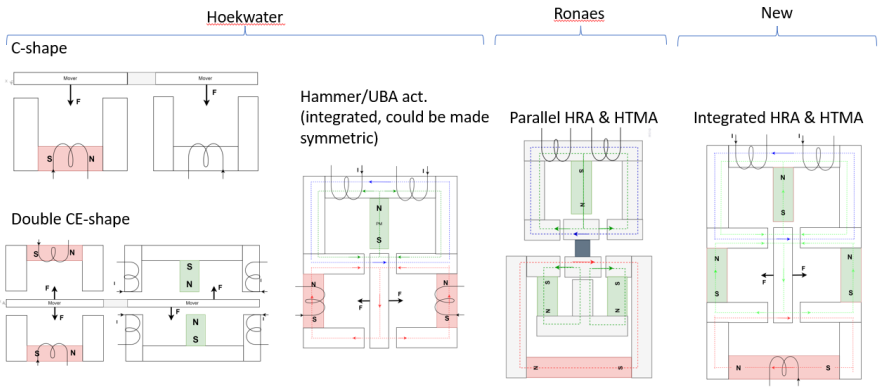

Figure A.3: Conceptual designs that are evaluated in more detail

For these 5 concepts, the K_{drive}, K_{tm} and k_a are evaluated in 3 steps.

1. Analytical derivation to show the basic force flux relation
2. MEC analysis in Matlab (flux losses are modeled at 30%)
3. 2D Comsol FEA (2D FEA overestimates the motor constants in line with the 30% flux losses found in the MEC analysis, later 3D FEA analysis shows that the flux losses are actually ~ 66% for the Dynamic HTMA.

Parallel C-shape

This is the most simple form which was proposed by [7] as a combined actuator. The parallel C-shapes can operate independantly but have a non-linear behaviour as can be seen in the plots below. The motor constant over the given range is low. This is also the only actuator that can only deliver force in a single direction as the reluctant forces always attract. The 2D FEA confirms the non-linear force flux relations and the motor constants are comparable. The actuator can be described by:

$$\mathbf{F} = \frac{\phi_{tm}^2}{\mu_0 A_g} + \frac{\phi_c^2}{\mu_0 A_g} = K_{tm}(x, B_{tm})\mathbf{B_{tm}^2} + K_{drive}(x)\mathbf{I_c^2} \tag{A.1}$$

.

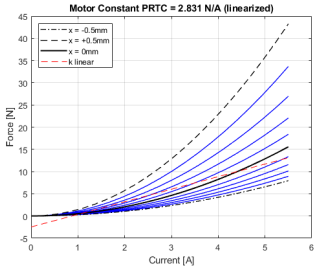

(a) Drive coil motor constant

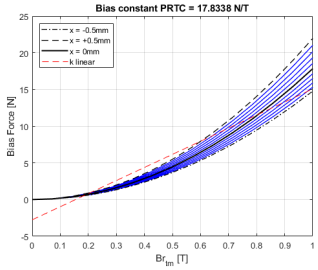

(b) Tunabl magnet motor constant

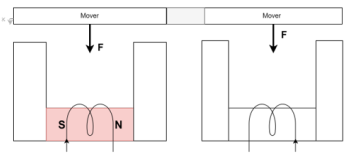

(c) C-shape concept

Figure A.4: Motor Characteristics of the C shape concept

Double CE-shape

This design mirrors the C-shape actuator on the other side of the mover. making it possible to create a linearized force but only over a small portion of the travel. In this concept it is possible to add permanent magnets because in the rest state, they cancel out each other and thus produce no net force

as is desired. The 2D FEA confirms the force flux relations and the motor constants are comparable. Note that the output this actuator is now dependent on the difference between the upper and lower half. Therefore, this actuator can be described by:

$$\begin{aligned}\mathbf{F} = K_{tm}(x, B_{tm}, B_{pm})\Delta\mathbf{B_m} + \\ K_{drive}(x, B_{tm}, B_{pm})\Delta\mathbf{I}\end{aligned} \tag{A.2}$$

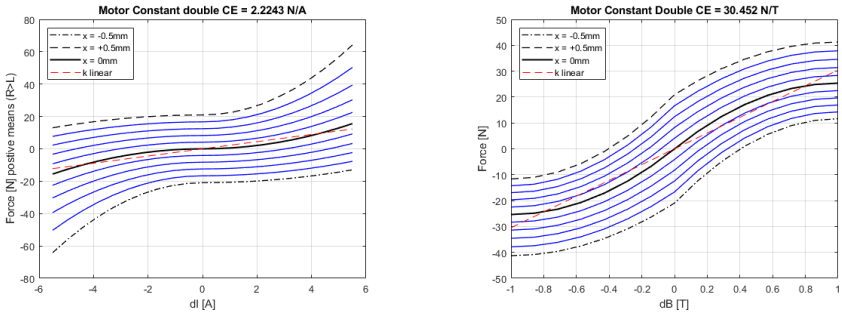

(a) Drive coil motor constant (b) Tunabl magnet motor constant

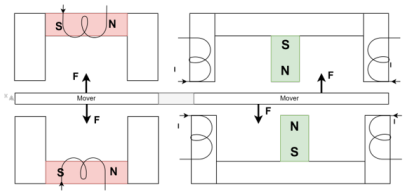

(c) C-shape concept

Figure A.5: Motor Characteristics of the double-CE shape concept

Uneven Bias Actuator

In this design the top half can be seen as the standard HRA and the top half of the double C-shape. The fluxes from the TM components are again related to the difference between left and right TM. The motor constant for the drive coil is linear as expected. However the TM force flux relation shows strange behaviour. This is because when the mover is not centered and the Magnetic fields of the TM's are not equal, the flux can shortcut the mover through the top loop. The motor constant of the drive coil also gets affected by the TM tuning state as the TM flux also acts as a bias flux. This actuator can be described by:

$$\mathbf{F} = K_{tm}(x, B_{tm})\Delta\mathbf{B_m} + K_{drive}(x, B_{tm})\mathbf{I} \tag{A.3}$$

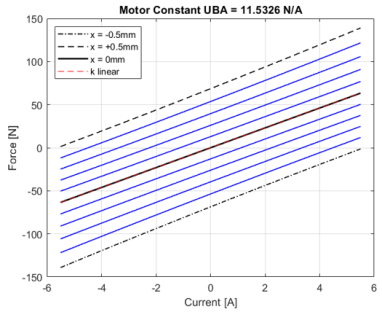

(a) Drive coil motor constant

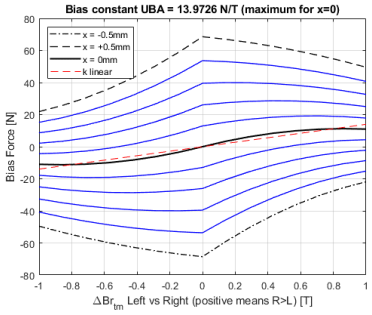

(b) Tunabl magnet motor constant

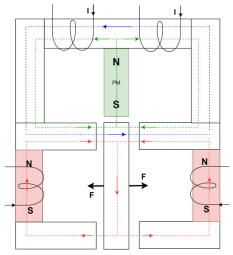

(c) Uneven Bias Actuator concept

Figure A.6: Motor Characteristics of the Uneven Bias actuator concept

Parallel HTMA & HRA

This design was proposed and validated by [2]. Both actuators have a linear force-flux relation and can be described by:

$$\begin{aligned}\mathbf{F} = K_{tm}(x, B_{tm}, B_{pm})\mathbf{B_{tm}} + \\ K_{drive}(x, B_{tm}, B_{pm})\mathbf{I_c} + \\ k_a(x, B_{tm}, B_{pm})x\end{aligned} \tag{A.4}$$

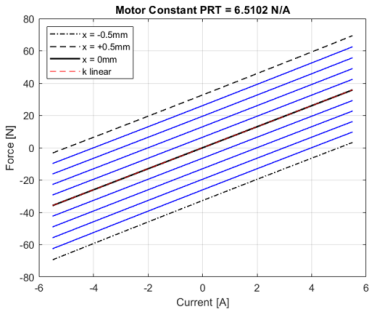

(a) Drive coil motor constant

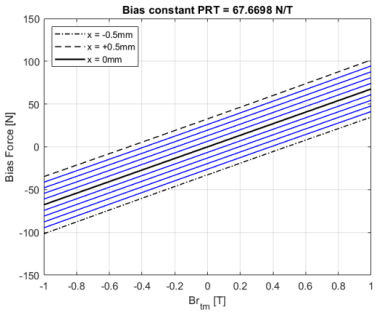

(b) Tunabl magnet motor constant

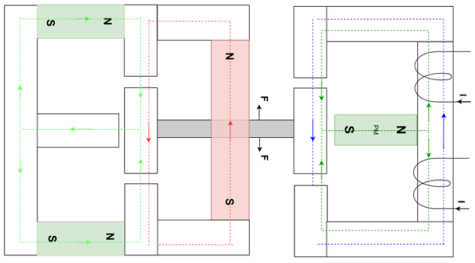

(c) Parallel HTMA & HRA concept

Figure A.7: Motor Characteristics of the Parallel HTMA & HRA concept

Dynamic HTMA This is the novel design presented in this research, it resembles the Parallel HTMA & HRA concept, but integrates the two circuits. This allows the bias flux from the HTMA to also work for the drive coil resulting in an increased K_{drive}. The 2D FEA confirms the linear force flux relations and the motor constants are indeed increased over the Parallel version. This actuator can also be described as:

$$\begin{aligned} \mathbf{F} = K_{tm}(x, B_{tm}, B_{pm})\mathbf{B_{tm}} + \\ K_{drive}(x, B_{tm}, B_{pm})\mathbf{I_c} + \\ k_a(x, B_{tm}, B_{pm})x \end{aligned} \tag{A.5}$$

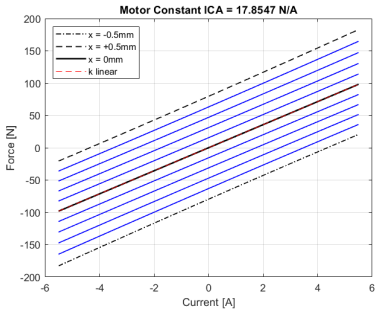

(a) Drive coil motor constant

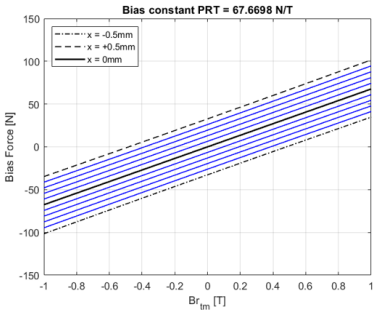

(b) Tunabl magnet motor constant

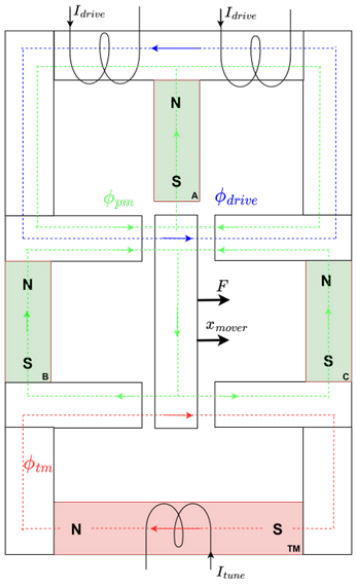

(c) Dynamic Hybrid Tunable Magnet concept

Figure A.8: Motor Characteristics of the Dynamic HTMA concept

Conclusion

The results are summarized quantitatively summarized in table **??**. 3 main conclusions are drawn:

- The Parallel C-shape actuator is simple but limited in capability and efficiency.
- The opposing TM's for the Uneven Bias actuator are complex and also inefficient due to a large part of the flux short-cutting the mover.
- Integration of the HTMA and HRA circuits almost doubles the drive coil motor constant over the parallel version.

Due to the reasons above, the choice was made to continue with the Dynamic HTMA concept.

	Bias motor constant	Coil motor constant	Linearity bias	Linearity coil	Force direction	Complexity
Parallel C-shape	low	low	non-linear	non-linear	single	Simple
Double CE-shape	low	low	non-linear	non-linear	bi-directional	Complex
Uneven Bias Actuator	low	mid	non-linear	linear	bi-directional	Complex
Parallel HTMA & HRA	high	mid	linear	linear	bi-directional	medium
Dynamic HTMA	high	high	linear	linear	bi-directional	medium

A.3. Actuator Characterization in 3D FEA

The force-current relation of the drive coil, the force-flux relation of the TM, and the actuator stiffness are shown in figure **??**. Both are plotted for a range of mover positions in the range $-0.2mm < x_{mover} < 0.2mm$. Note that the FEA results show some non-linearity especially at higher fluxes and the outer position ranges. Because this is a proof of concept, very high accuracy is not required. Therefore for simplicity it is chosen to reduce the motor constants to a linear fit. Table A.1 shows the values of the motor constants and the RMS errors due to the linearization. The maximum combined force output at $I_{drive} = 3A$, $B_{tm} = 1T$ and $x_{mover} = 0.2mm$ is $48.6N$

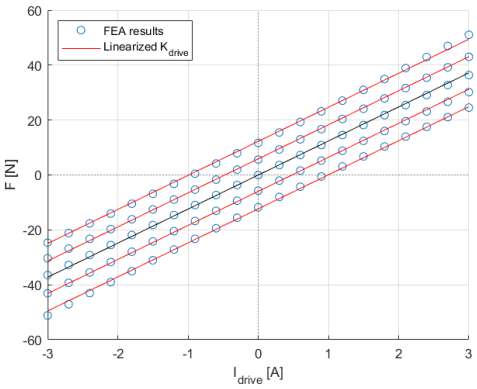

(a) Force-Current relation

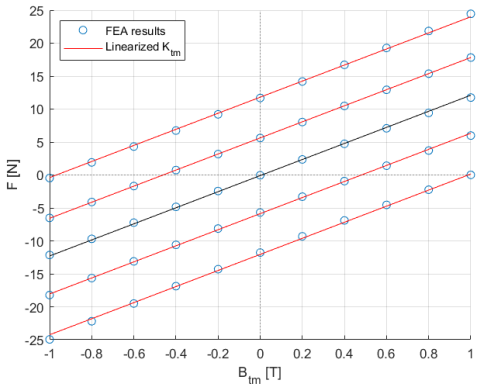

(b) Force-flux relation

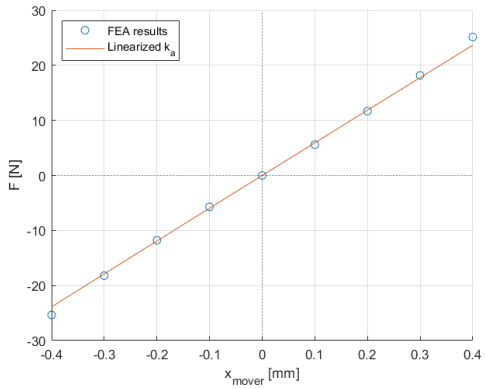

(c) Actuator stiffness

Table A.1: Actuator characteristics found by COMSOL 3D FEA

Symbol	Value	Linearization RMSE	Comment
K_{drive}	$12.4N/A$	$0.51N$	Motor constant
K_{tm}	$12.2N/T$	$0.19N$	Motor constant
K_a	$-59.4kN/m$	$0.74N$	Actuator stiffness
x_{max}	$\pm 0.2mm$		movement range
$F_{max,x=0}$	$\pm 48.6N$		Combined Force range

B. Experimental Setup

Unfortunately, due to time constraints, it was not possible to build a test setup and to execute an experiment in this thesis project. However, practical designs were made and some components were fabricated.

B.1. Experiment plans

The goal of the experiment was to validate the design and to show any shortcomings that may not have been discovered during modeling and simulations. Especially the dynamics are an interesting part that require significant tuning of the controllers.
The following general steps were planned:

- **Experiment setup and familiarization**
  The concept of separating the low- and high-frequency force components could have been tested with the parallel HRA & HTMA actuator setup that was built by E. Ronaes. The controllers for his setup and the new actuator would be identical and only require tweaking of parameters because of the different motor constants. It is therefore a perfect first step to get familiar with the electronic and software aspect of the experiment. Data acquisition can be adjusted and analyzed to provide the desired outputs. Figure B.1 shows the setup. The performance comparison that is done in the analysis section of chapter 3 can be repeated to show the benefit of this concept.

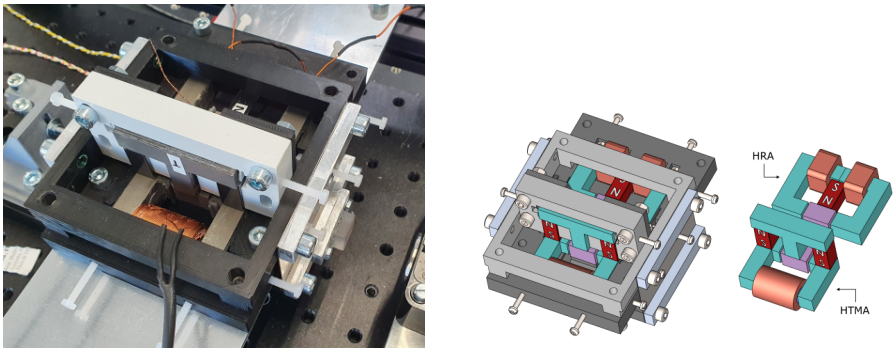

(a) A picture of the parallel HRA & HTMA actuator setup.

(b) The CAD design of the parallel HRA & HTMA actuator setup.

Figure B.1: Experimental Setup of E. Roneas [2]

- **Build new setup**
  The design was made to be compatible with the setup of Ronaes [2]. It should be possible to re-use the base plate, flexures, and electronic setup.
- **Characterize new setup**
  To accurately control the actuator, the characteristics must be identified. This step also verifies results from the simulation. Most important are the motor constants, (negative) stiffness, and losses. Finally, the hall and force sensors must be calibrated. The new values must be implemented in the Labview FPGA code.
- **Repeat experiment with new setup**
  After correctly setting up the actuator mechanically and control wise. The performance comparison can be done again. The experience gained from practicing on the old setup should make this step much easier. It is expected to see a similar reduction in heat reduction between

the combined actuation and the a single HRA. The goal would be to recreate a similar plot as the one below with experimental data:

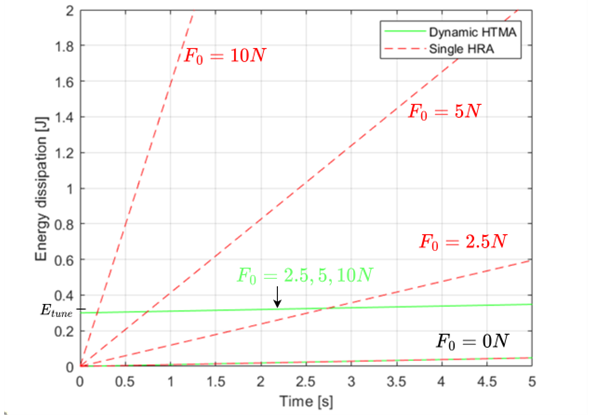

Figure B.2: The energy dissipation over time of both actuators following the reference signal with $F_0 = 0, 2.5, 5$ and $10N$ from FEA simulation.

B.2. CAD model

Because the goal is to validate the design and to show any shortcomings that may not have been discovered during modeling and simulations, the requirement for the setup is that it is repeatable. The accuracy of the actuator is mostly a control aspect and not the most important in this phase. The Design approach was to use as many existing components as possible, The AlNiCo 5 Magnet and its tuning coil and all of the supporting electronics can be carried over. he Yokes, Permanent magnets, drive coil, hall sensors and the support structure around it are specific for this design. The yokes are designed to fit into a 3D-printed casing that has bolts on one side to push all components to one side. By applying this force, the friction should hold all other components in place.

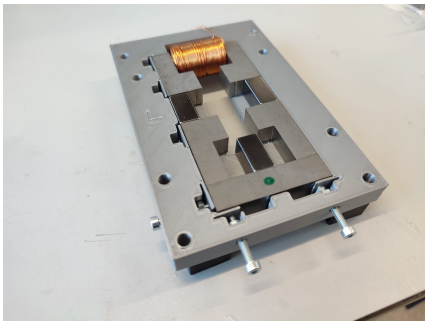

(a) Dynamic HTMA without the mover in place.

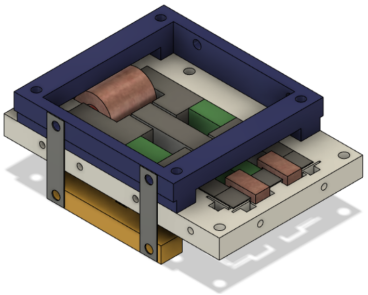

(b) The CAD design of the Dynamic Hybrid Tunable Magnet actuator with support structure and flexures.

Figure B.3: The intended Experimental setup of the Dynamic HTMA

B.3. Yokes

Eddy currents in iron yokes can have a significant effect on the accuracy of an actuator. The tuning of the magnet becomes rate dependent and unpredictable. It is widely known that using laminated thin sheets that are electrically isolated can greatly reduce these effects. Wiersema studied this effect for Magnetization state tuning and concluded that laminating the yokes significantly decreased dynamic effects during tuning. This helps the repeatability and accuracy of the controller [6]. It was therefore chosen to laminate the yokes with 0.35mm thick M235-35A Magnetic steel sheets. This material is specially designed for low-voltage, high-frequency transformers to reduce losses in the material. To reduce production costs, the yokes are designed in such a way that there only 2 different geometries that can be oriented in such a way that it completes the flux paths. Four L-shaped corner pieces and one simple straight part that is the mover as well as the part where the drive coil is wrapped around.

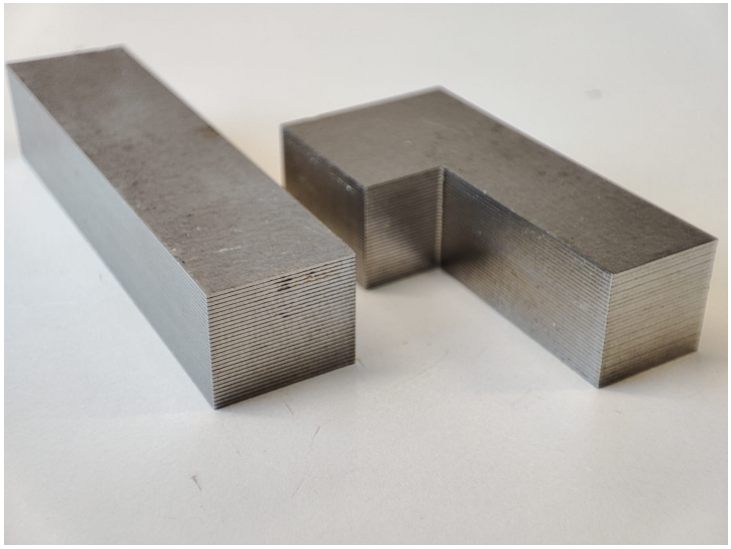

Figure B.4: The two different yokes, laminated from 0.35mm thick sheets of M235-35A Magnetic Steel

C. Potential Efficiency gains

The contents of this appendix where made prior to the research to show the potential benefit of the chosen strategy to split the low and high-frequency outputs of an actuator.
To provide a first indication of how much a combined actuator can improve the efficiency of a conventional HRA, simple first-order calculations are done on an example actuator.
The example used is the Deformable mirror Hybrid Reluctance Actuator as developed by TNO [8] and shown in figure C.1.

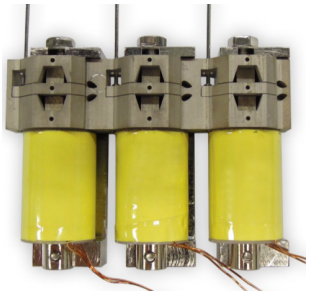

Figure C.1: A strip of 3 prototype actuators as developed by TNO [8]

Table C.1: example actuator

Example Actuator [3]		
Symbol	**value**	**Comment**
k	52 $[N/A]$	Motor constant
α_{act}	38 $[N/\sqrt{W}]$	Actuator efficiency
R	2.4 $[\Omega]$	Coil resistance
F_{range}	± 8 $[N]$	Force bandwidth

The relation between heat dissipation and Force of this actuator, can be calculated using the motor constant as described in [12], and Joule's law. Combining these equations we can the heat dissipation - Force relation equation C.3. Where α_{act} is the actuator efficiency which contains the physical parameters of the actuator design from equation C.1.

$$k = \frac{F}{I} = \lambda n \frac{B_r A_m}{l_{g1} + l_{g2}} \tag{C.1}$$

$$P = I^2 R \tag{C.2}$$

$$P = \frac{F^2}{\alpha_{act}^2} \tag{C.3}$$

Although the Force current relation is linear, the heat dissipation rises exponentially with force input. Therefore, for heat dissipation, it is desirable to have the actuator act as close to its equilibrium as possible. When evaluated for 0-10 N, the actuator characteristics are visualized in figure C.2

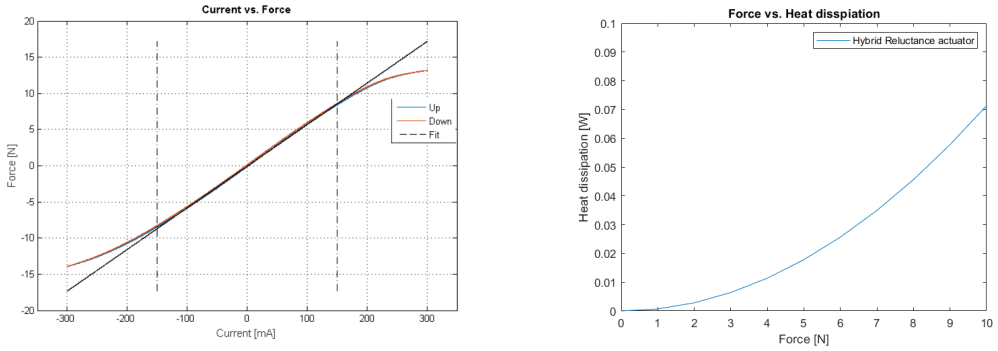

(a) (b)

Figure C.2: (a)Force-Current relation of the example actuator [8] (b) The Heat dissipation versus Force of the example Actuator based on equation C.3

As a use case, consider a time-based reference signal where A is the amplitude, f the frequency, and F_{bias} the constant bias component. It is plotted over a 5-second time interval in figure C.3a with 2 levels of F_{bias}, 0 and 5 N. An amplitude of 1N and frequency of 3Hz are used.

$$F_{ref} = Asin(2\pi f t) + F_{bias} \tag{C.4}$$

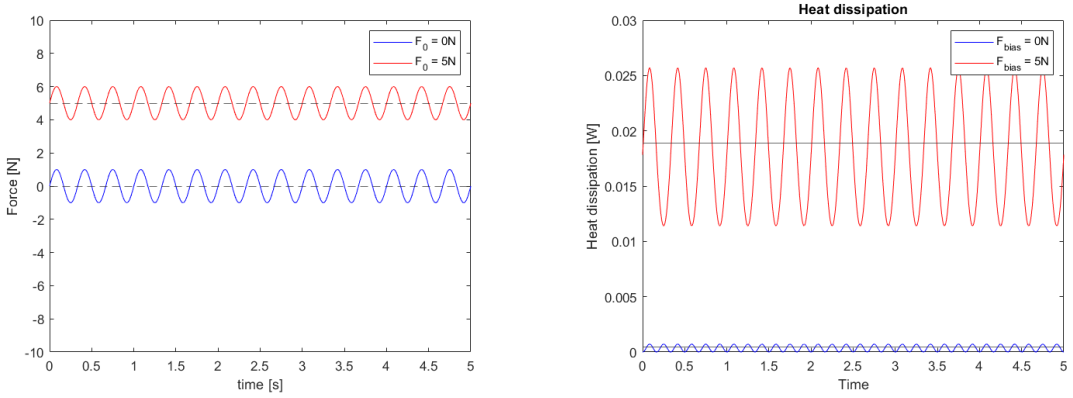

(a) (b)

Figure C.3: (a)Force Reference signal plotted over time (b) The heat dissipation of the example actuator for the reference signal

Although the increase in bias force looks benign, the actuator now operates constantly between 4 and 6 N dissipating roughly 43 times more heat (RMS).

Suppose the reference signal is split into a dynamic part that is taken care of by the coils of a reluctance actuator and a constant part that is provided by the tunable magnet. In a series configuration shown in figure A.1a, the fluxes created by both parts can be added to resemble the reference signal.

$$F_{coil} = Asin(2\pi f t) \tag{C.5}$$

$$F_{TM} = F_{bias} \tag{C.6}$$

$$F_{Comb} = F_{coil} + F_{TM} \tag{C.7}$$

The magnet tuning only requires a short pulse of current to achieve it's desired tuning state. If the Force bias is constant for t ≫ BTI, the tuning energy is negligible and the continuous heat dissipation of the actuator is reduced by 97% for this specific case.

When the force bias changes, the magnet has to be tuned, if this tuning interval is shorter than a pre-specified BTI, the combined actuator is likely to be less efficient.
For this actuator and the case where t ≫ BTI, the efficiency gain versus the force bias as a fraction of the original amplitude is shown in figure C.4. When the Force bias is equal to the Amplitude of the dynamic force, the heat dissipation could be reduced by 70% by using the combined actuator.

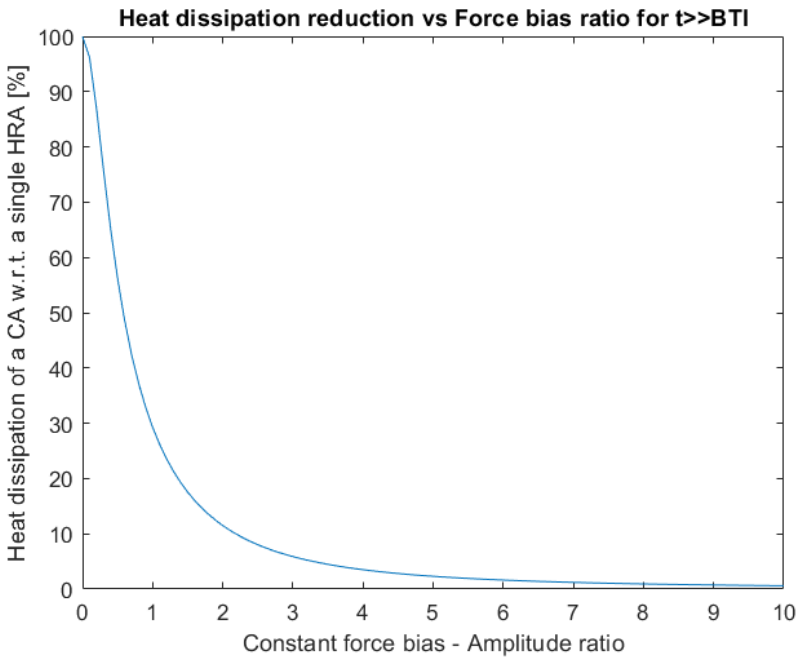

Figure C.4: The heat dissipation

D. Extended Literature review

D.1. Bias Force Actuators

As identified in the research gap, a bias force component with low energy input is desired to increase the overall efficiency of an actuator. One application where a constant bias force is desired is gravity compensation. These gravity compensators are usually applied in vibration isolation systems where the end effector, for example, a high-precision metrology instrument, must be isolated from external disturbances. Instead of rigid connections to a base, a low-stiffness connection is made to reduce the transmissibility from the environment to the end-effector. This however poses the problem that the mass of the end-effector (often significant) still has to be supported. The gravitational forces are therefore counteracted by a low stiffness actuator, hence the name 'gravity compensator'. The gravitational force of an object is static and could be seen as the constant bias force that is mentioned in section **??**. One example of this is proposed in the work of Hol [9]. This actuator provides a static force of $85N$ with permanent magnets and a voice-coil type actuator can add a dynamic force of $\pm 20N$. The layout is shown in figure D.1. The bias force component is static, this limits the applicability of this actuator.

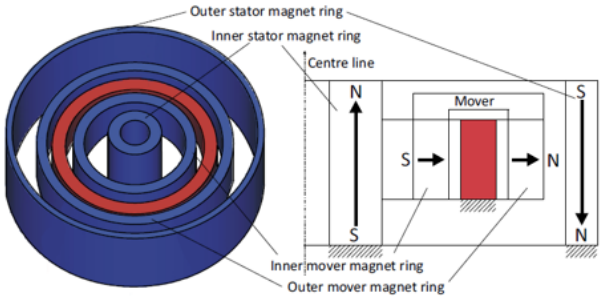

Figure D.1: A voice-coil type actuator with added permanent magnets to provide a static force.[9]

A patent by Ji [10] provides a solution to this limitation. The design presented in figure D.2, is very similar to the design of Hol with an inner magnet ring and a Lorentz actuator. However, in this design, the inner magnets can be brought closer to the mover. This way, the static force component is made adjustable. This device is in principle similar to the proposed combination of HRA and TMA but there are drawbacks to this design. The Lorentz-Force actuators are known to have lower Force densities which makes them less efficient and the moving parts associated with the adjustment mechanism are prone to wear and require maintenance. This is undesirable in space or vacuum environments.

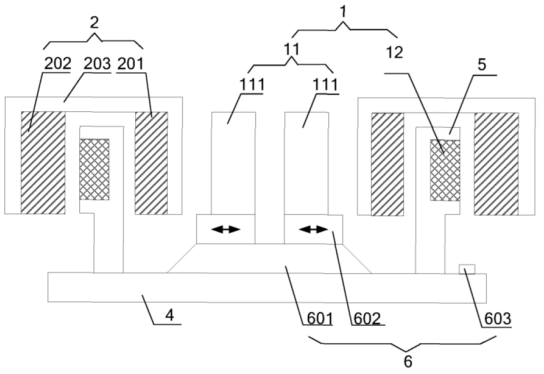

Figure D.2: A magnetic gravity compensator with an adjustment mechanism to vary the static force component [10]

A very different technology called 'PIrest', is focused on Hysteresis behavior in Piezo-electric actuators. Although the physical mechanisms are different, Reiser et al resemble the Magnetization state tuning process[11]. They describe how a Piezo can maintain its last position without an offset voltage. The mechanism is based on ferroelectric domain orientations of soft PZT ceramics. The Mechanical strain is increased when a voltage is applied. After the voltage is removed, the strain reduces to a remanent strain. This remanent strain can be tuned much like the remanent flux density of a permanent magnet. (Figure D.3b)
Combining this with a normal Piezo-electric actuator can create a similar dynamic and static force component split. In this case, the actuator is combined in a series arrangement. A parallel arrangement would lead to over-constraints due to the high stiffness of the actuators. (Figure D.3a)

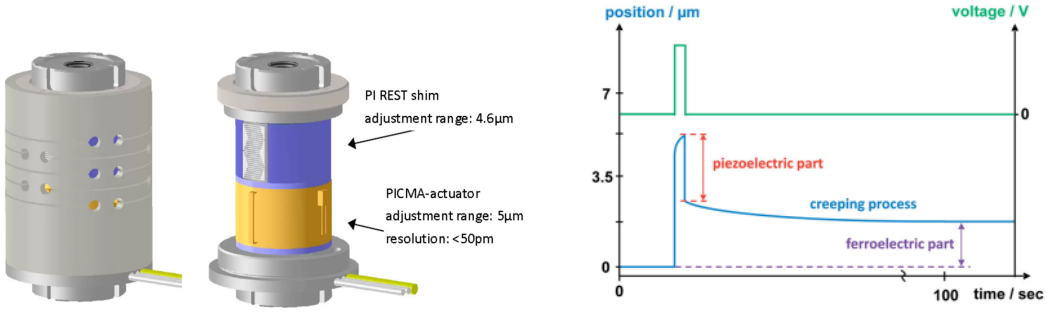

(a) (b)

Figure D.3: (a)A CAD design of the Combined (series) Actuator (b) The Heat dissipation versus Force of the example Actuator based on equation C.3 [11]

D.2. Combined actuator designs by Hoekwater [1]

Hoekwater started his thesis with a similar goal to design a combined HRA and TMA actuator. During his thesis, his focus shifted towards designing for a linear force-flux relation, but there are still relevant results that are summarized in this section.

D.2.1. Recoil line actuator

Instead of combining 2 actuators a variation of the TMA could be used to achieve high-frequency actuation. Due to the linearization of the recoil lines, it is possible to shift the operation point of the

magnet over the recoil lines. As a result, the higher frequencies could be achieved by shifting back and forth over the recoil lines while keeping the same remnant magnetization state. Demagnetization only occurs when the load line reaches the major loop hysteresis curve. Therefore the maximum Force amplitude of a dynamic signal to be followed is limited. This is visualized in figure D.4.

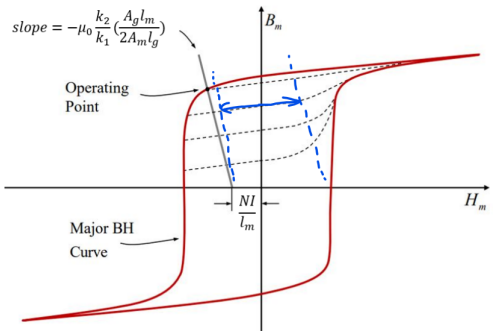

Figure D.4: If the operating point remains within the given boundaries, the magnetization state of the magnet does not change.

To answer the question, if a recoil line actuator is more efficient than adding a separate RA to a TMA, The following relation could be used to estimate the relation between Magnetic flux density ΔB and the coil current ΔI where K is the slope of the load line, n the number of coil windings, l_m the magnet length and μ_{rec} the slope of the recoil line.

$$\Delta B = \frac{\mu_0 \mu_{\text{rec}}\, k}{k + \mu_{rec}\mu_0} \frac{n}{l_m} \Delta I = K_{BI,recoil} \Delta I \tag{D.1}$$

$$\Delta B = \frac{\mu_0 N}{2 l_g} \Delta I = K_{BI,RA} \Delta I \tag{D.2}$$

Comparing $K_{BI,recoil}$ and $K_{BI,RA}$ will show the relation between ΔB and ΔI of each setup in figure D.5. This is for a C-shaped actuator with a 10x10mm magnet cross-section area and for small changes on the same recoil line only. On average, adding a separate RA will be 6x more efficient than using a recoil line actuator, only considering ohmic losses.

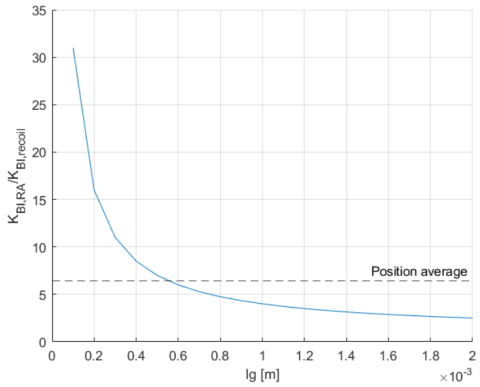

Figure D.5: Ratio between current and flux for both actuators for different air gap lengths to show the energy gain that can be obtained by using a RA [1]

D.2.2. Combinations of HRA and TMA

Hoekwater's method to find an optimal combination of HRA and TMA was to first find the most optimal HRA and the most optimal TMA configurations on their own and then combine these.

For the Tunable magnet actuator, 6 different layouts were considered. These layouts are shown in figure D.6. For each layout, a lumped parameter model is analyzed and FEA is used to calculate the loss factor. Based on these results, the E-shape layout proved to be the most promising configuration as it has the highest force/energy values and the lowest stiffness.

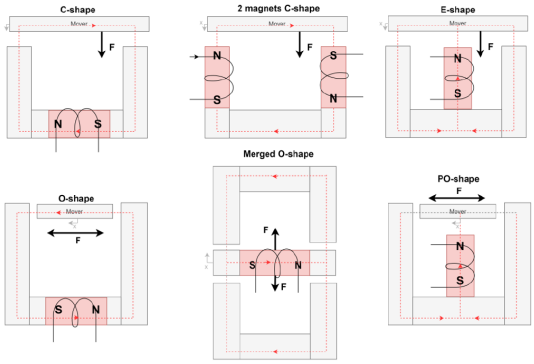

Figure D.6: Overview of the different TMA configurations considered in this project. The TMs are denoted in red, and the iron cores in white. The main flux paths are visualized by dashed red lines. [1]

For the Reluctance Actuators, 7 different layouts were considered. These layouts are shown in figure D.7. The generation of a bias flux improves the efficiency and a linear force-flux relation is desired. It's most efficient if this bias flux is provided by a PM. Based on this quantitative analysis, the HRA type is the most promising one to use in combination with a TMA.

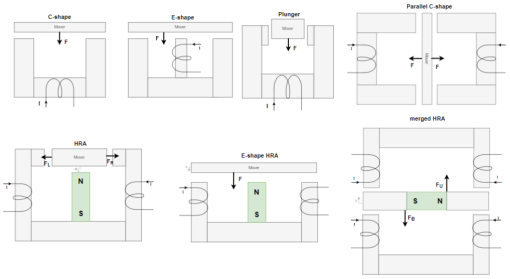

Figure D.7: Overview of the found RA configurations [1]

To combine these optimal HRA and TMA designs, non-magnetic material is used to combine the multiple mover elements into a single mover. The result is the so-called 'Hammer' setup as shown in figure D.8. This actuator is symmetric (therefore no moments are generated) and it can deliver force in both directions. Depending on the direction of the force needed for the static forces, the top or bottom E-shape TMA should be used.

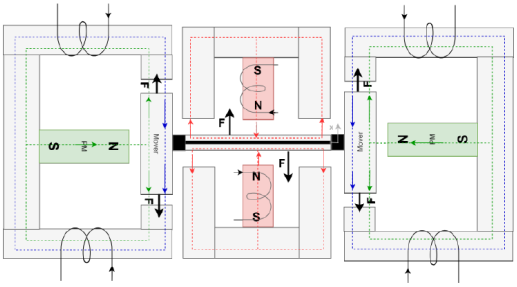

Figure D.8: A possible combination of the optimal HRA and TMA actuators [1]

D.2.3. Combined Actuator Control

Although the focus of Hoekwater was on the design, he did propose some methods of controlling the combined actuator. Figure D.9 shows a top level controller. With the use of filters, the reference signal can be split up into 2 signals, one bias signal, and one dynamic force signal.

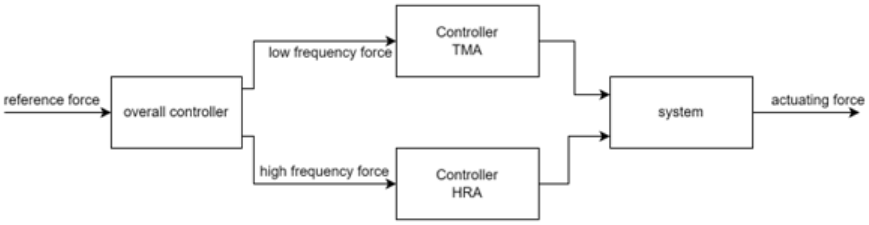

Figure D.9: [1]

D.3. Combined actuator design by Ronaes [2]

To remedy the inherent overshoot of the TMA that is mentioned in section **??**, Ronaes designed a parallel HRA and HTMA actuator that is shown in figure D.10 [2]. The idea is to attenuate the overshoot actively with a higher-bandwidth actuator (in this case an HRA). The HTMA design is based on that of Hoekwater and the HRA is designed to have a similar displacement range as the HTMA and their movers are rigidly connected to each other with non-ferromagnetic material to make a parallel type actuator. This design combines gives a lot of room for circuit optimization to achieve higher motor constants. This design should therefore be considered a good option to achieve combined actuation. It is however relatively large and has many components.

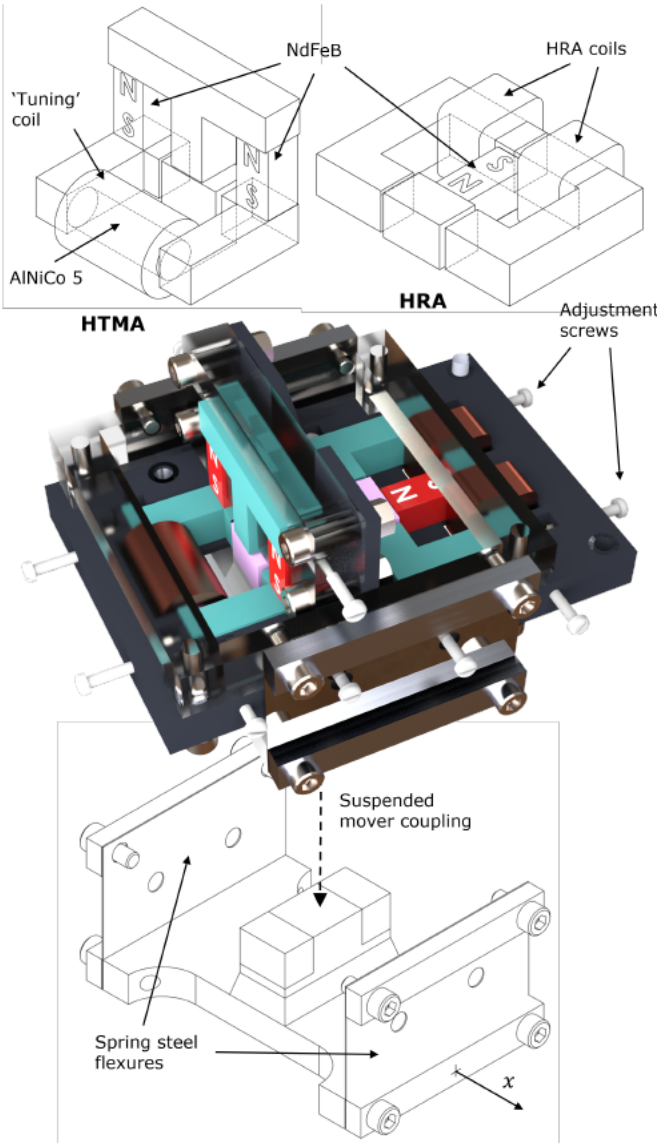

Figure D.10: Render of setup for a parallel configuration of the HTMA and an HRA of similar proportions. [2]

REFERENCES

[1] William B. Hoekwater, Endre Ronaes, and Hassan HosseinNia. Hybrid tunable magnet actuator: Design of a linearized force-flux tunable magnet actuator. *IEEE Transactions on Industrial Electronics*, pages 1–10, 2023.

[2] E P Ronaes. Tunable magnet actuators: Remnant magnetisation state and position control of a hybrid tunable magnet actuator, 2023.

[3] Thorsten Hüfner, Oliver Radler, Tom Ströhla, Thomas Sattel, Jasper Wesselingh, Alexander Vogler, and Dirk Eicher. A note on electromagnetic gravity compensation actuators based on soft electro-permanent magnets for adjustable reluctance force. *Proceedings of the 17th International Conference of the European Society for Precision Engineering and Nanotechnology, EUSPEN 2017*, pages 149–150, 2017.

[4] Romano Meijer. Modeling and prototyping of a tuneable magnet actuator for quasi-static and low-frequency dynamic applications. pages 1–25, 2020.

[5] Edward P. Furlani. *Permanent magnet and electromechanical devices*, volume 148.

[6] J D Wiersema. Tunable magnet actuators: Hysteresis modelling for efficient and accurate magnetization state tuning, 2022.

[7] S.G. Viëtor. Tunable magnets: Modeling and validation for dynamic and precision applications. *Thesis Topology*, pages 5–7, 2018.

[8] Stefan Kuiper, Niek Doelman, Evert Nieuwkoop, Ton Overtoom, Tjeerd Russchenberg, Martijn van Riel, Justin Wildschut, Max Baeten, Jet Human, Helma Spruit, Sanneke Brinkers, and Matthew Maniscalco. Electromagnetic deformable mirror development at tno. volume 9912, page 991204. SPIE, 7 2016.

[9] SAJ Hol. *Design and optimization of a magnetic gravity compensator*. 2004.

[10] Qingsheng Hanchuan Ji, Chen. Adjustable magnetic buoyancy gravity compensator - patent.

[11] J. Reiser and H. Marth. Pirest technology - how to keep the last position of pzt actuators without electrical power. In *ACTUATOR 2018; 16th International Conference on New Actuators*, pages 1–4, 2018.

[12] Schmidt R M, Schitter G, Rankers A, and van Eijk J. *The Design of High Performance Mechatronics*. IOS Press, 3rd edition, 2020.

[13] Twelve projects get a go through the open technology programme, Dec 2022.

[14] Andelko Katalenic. *Control of reluctance actuators for high-precision positioning*. 2013.

[15] Rachel Bowens-Rubin, Philip Hinz, Stefan Kuiper, and Daren Dillon. Performance of large-format deformable mirrors constructed with hybrid variable reluctance actuators ii: initial lab results from flash. page 69. SPIE-Intl Soc Optical Eng, 7 2021.

[16] A Knaian. Electropermanent magnetic connectors and actuators : devices and their application in programmable matter. page 208, 2010.

[17] Shingo Ito, Stefan Troppmair, Bernhard Lindner, Francesco Cigarini, and Georg Schitter. Long-range fast nanopositioner using nonlinearities of hybrid reluctance actuator for energy efficiency. *IEEE Transactions on Industrial Electronics*, 66:3051–3059, 2019.

[18] John R. Brauer. *Magnetic Actuators and Sensors*. Wiley-IEEE Press, 2014.